Publishing House
AKAPIT

COMPUTER METHODS IN MATERIALS SCIENCE

Informatyka w Technologii Materiałów

Vol. 15, 2015, No. 2

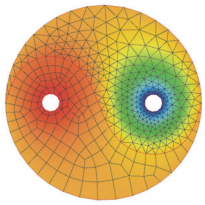

RECENT AND FUTURE DEVELOPMENTS IN FINITE ELEMENT METAL FORMING SIMULATION

S. ANDRIETTI[1], J.-L. CHENOT[1,2]*, M. BERNACKI[2], P-O BOUCHARD[2], L. FOURMENT[2], E. HACHEM[2], E. PERCHAT[1]

[1]Transvalor, 694 Avenue du Dr. Maurice Donat, 06255 Mougins Cedex, France
[2]CEMEF, Mines Paristech, B.P. 207, 06904 Sophia Antipolis Cedex, France
**Corresponding author: jean-loup.chenot@mines-paristech.fr*

Abstract

After more than 40 years of development, finite element metal forming simulation has reached a high level of maturity. After a short mechanical and thermal introduction, the main scientific and technical developments are briefly described. We consider numerical issues, such as adaptive remeshing or parallel computing; coupling phenomena for a more realistic simulation, such as thermal and metallurgical coupling, with a special emphasis on modeling of microstructure evolution; the use of optimization for forming processes or for parameters identification. Finally the main potential future research fields for the next 10 years are outlined: process stability and stochastic approaches, more effective massively parallel computing and extension of the application to generate the whole "virtual factory".

Key words: Plasticity, finite element modeling, metal forming simulation

1. INTRODUCTION

Finite element simulation of metal forming processes started at the beginning of the 70's, mainly in academic laboratories. We can quote the 2D approaches treating: hydrostatic extrusion by Iwata et al. (1972), hot rolling by Cornfield and Johnson (1973), analysis of relative slip on the tools by Lee and Kobayashi (1973), and large deformations of viscoplastic materials by Zienkiewicz and Godbole (1974). In the 1980's the use of simulation codes started for industrial forming applications, while 3D forging developments started in laboratories by Surdon and Chenot (1987). Since these early developments, commercial finite element computer codes are developed and maintained in several software companies (Transvalor, SFTC, *Simufact Engineering GmbH*, Quantorform, etc.) which favor their diffusion in large and medium enterprises. Simulation is widely recognized by the engineers as more complex processes can be treated with a realistic approach. As an example, we can list the availability of the main developments in FORGE®, a 3-D commercial code, as follows:

- 1995: automatic remeshing,
- 1996: element quality control,
- 1997: parallel computing,
- 2002: heat treatment, quenching,
- 2003: deformable tools,
- 2005: coupling with metallurgy,
- 2007: thermal regime in tools, multi body forming,
- 2009: process optimization,
- 2014: three-dimensional modeling of induction heating.

ISSN 1641-8581

The main purpose of the paper is to review and analyze the present state of the numerical and physical approaches for treating a wide range of metal forming problems and present some examples, most of them being obtained from our FORGE® simulation software. Moreover some new challenges that are emerging will be discussed briefly.

2. MECHANICAL AND THERMAL FORMULATIONS

For a more complete introduction to numerical simulation of metal forming see Wagoner and Chenot (2001).

2.1. Updated lagrangian, eulerian or ALE

The mechanical equations are generally expressed with an integral formulation in term of density ρ, acceleration γ, virtual velocity v^*, stress tensor σ, virtual strain rate $\dot{\varepsilon}^*$ and stress boundary condition τ, on a part of the boundary $\partial\Omega_c$ of the current configuration Ω :

$$\int_{\Omega} \rho\gamma \mathrm{v}^* \mathrm{dV} + \int_{\Omega} \sigma : \dot{\varepsilon}^* \mathrm{dV} - \int_{\partial\Omega_c} \tau \mathrm{v}^* \mathrm{dS} = 0 \quad (1)$$

For processes which can be considered as mostly steady-state, such as rolling, extrusion or wire drawing, an Euler description can be utilized where the domain Ω is assumed to be fixed. In this case, the major problem is to determine the free surface and to take into account memory effects, e. g. work hardening, for computing the stress tensor field.

In most non-stationary metal forming applications the inertia contribution can be neglected in equation (1) and an updated lagrangian approach is preferred, which corresponds to a first order integration scheme for the domain, the stress tensor and memory variables. On the domain Ω^t at time t, equation (1) is approximated by:

$$\int_{\Omega^t} \sigma^{t+\Delta t} : \dot{\varepsilon}^* \mathrm{dV} - \int_{\partial\Omega_c^t} \tau^{t+\Delta t} \mathrm{v}^* \mathrm{dS} = 0 \quad (2)$$

Material points, stress tensor and memory variables (here the equivalent strain $\bar{\varepsilon}$) are updated according to:

$$\begin{aligned} x^{t+\Delta t} &= x^t + \Delta t v^t \\ \sigma^{t+\Delta t} &= \sigma^t + \Delta t \dot{\sigma}^t \\ \bar{\varepsilon}^{t+\Delta t} &= \bar{\varepsilon}^t + \Delta t \dot{\bar{\varepsilon}}^t \end{aligned} \quad (3)$$

The ALE (Arbitrary Lagrange Euler) formulation can be utilized when the boundary of the domain varies slowly, for example in ring rolling. A numerical velocity field v_{ALE} is defined in the domain, which is different from the material velocity. The material derivative for any variable is replaced by the ALE derivative in the moving frame. As an example for the equivalent strain $\bar{\varepsilon}$ we have:

$$\frac{d_{ALE}\bar{\varepsilon}}{dt} = \dot{\bar{\varepsilon}} + (v - v_{ALE}) grad(\bar{\varepsilon}) \quad (4)$$

The conservation of the boundary surface must be imposed by the following condition on the normal vector n :

$$(v - v_{ALE}).n = 0 \quad (5)$$

2.2. Constitutive modeling

The first approaches of FE modeling of forming processes were based on a viscoplastic or rigid plastic behavior. In order to be able to model also the elastic component of the deformation, and more specifically to predict the residual stresses, an elastic viscoplastic or elastoplastic approach is selected where the strain rate is decomposed into an elastic part $\dot{\varepsilon}^e$ and an irreversible contribution $\dot{\varepsilon}^p$:

$$\dot{\varepsilon} = \dot{\varepsilon}^e + \dot{\varepsilon}^p \quad (6)$$

The elastic law is written with the Jauman derivative in order to keep material objectivity:

$$\frac{d_J \sigma}{dt} = \lambda tr(\dot{\varepsilon}^{\mathrm{e}}) + 2\mu\dot{\varepsilon}^{\mathrm{e}} \quad (7)$$

Where λ and μ are the usual Lamé coefficients. The viscoplastic contribution is often expressed by an isotropic Norton power law of the form:

$$\dot{\varepsilon}^p = \frac{1}{K}\left\langle (\bar{\sigma} - R) / K \right\rangle^{\frac{1}{m}-1} \sigma' \quad (8)$$

We have introduced σ' the deviatoric stress tensor, $\bar{\sigma}$ the usual equivalent stress, K the material consistency and m the strain rate sensitivity.

More complicated constitutive equations are used to take into account anisotropy according to

Hill (1948) or Barlat and Lian (1989) theories, or to deal with porous materials.

2.3. Contact, friction and wear

Contact occurs between the work-piece and the tools, between different parts of the tools or in the case of multi materials forming. For two bodies with velocities v_a and v_b the non-penetration condition is expressed as:

$$(v_a - v_b)n = \Delta vn \leq 0 \tag{9}$$

Relative sliding between the two bodies generates a friction tangential stress τ_f on the interface $\partial\Omega_c$, that can be given for example by a Coulomb-Norton law:

$$\tau_f = -\mu_f(\sigma_n)\Delta v / |\Delta v|^{1-p_f} \tag{10}$$

Where μ_f and p_f are friction coefficients and σ_n is the normal stress component.

Wear is a complicated physical phenomenon, the abrasion contribution depends on the normal stress, the relative velocity and the hardness H_V. It is often represented by a generalization of the Archard and Hirst (1956) law:

$$\delta_W = K_W \cdot \int \frac{\sigma_n \cdot \Delta V}{{H_V}^{m_W}} \cdot dt \tag{11}$$

Where δ_W is the amount of wear, K_W and m_W are physical parameters associated with the material.

2.4. Damage

Fracture prediction during materials forming processes has been of utmost interest in the scientific and engineering community in the past century. Indeed, understanding and modeling ductile damage mechanisms remains a major issue to get defect-free products. Many phenomenological and micromechanical models were developed during the last twenty years to predict ductile fracture. These models are usually validated for given loading path (most of the time under monotonic loading) and specific materials, and their ability to be extended to other configurations – in terms of loading and materials – is often questionable. Enhancing these models is necessary for their application to real industrial processes. This requires accounting for non-proportional loadings (Bouchard et al., 2011; Gachet et al., 2014) and for low stress triaxiality ratios. Recent studies also showed the influence of the third invariant of the deviatoric stress regarding ductile fracture critical strain. The Lode parameter was introduced by many authors in classical ductile damage models to get a better prediction of the influence of the stress state on ductile fracture (Nahshon & Hutchinson, 2008; Cao et al., 2014). New mathematical formulations and numerical solution strategies dedicated to efficient modeling of continuum ductile damage and its transition to discontinuous fracture are also important. The use of non-local formulation coupled with anisotropic mesh adaptation is an efficient way to predict failure accurately and to model the transition between continuous damage approaches to discontinuous fracture (El Khaoulani & Bouchard, 2012). In the future, the modeling of ductile failure at the microscale appears to be essential to get a better understanding of microstructural heterogeneities on ductile fracture for complex loading paths. Such microstructural simulations require being able to mesh complex microstructures and to model nucleation, growth and coalescence mechanisms for large plastic strain and complex loading paths. In (Roux et al., 2013; Roux et al., 2014) a new approach based on level set functions and anisotropic mesh adaptation is presented (see section 7 for more details). It is possible to simulate nucleation and void growth mechanisms when a matrix containing hard inclusions is submitted either to tension or to shear loading.

2.5. Heat equation

The classical integral form of the heat equation is written:

$$\int_{\Omega'} \rho c\dot{T} w dV + \int_{\Omega'} k\,grad(T)\,grad(w) dV - \int_{\Omega'} \dot{q}_V w dV + \int_{\Omega'} \phi_n w dS = 0 \tag{12}$$

Where w is a scalar test function, k is the thermal conductivity, $\dot{q}_V$ is the heat dissipated by plastic or viscoplastic deformation, ϕ_n is the heat flow on the boundary $\partial\Omega$, which comes from conduction, friction or radiation.

3. SPACE AND TIME DISCRETIZATION

3.1. Tetrahedral elements

In metal forming simulation by the Finite Element method (FEM), the mesh is progressively dis-

torted and the resulting accuracy decreases so that the mesh must be regenerated periodically. Therefore the work-piece must be discretized by elements which are convenient for initial meshing and *automatic remeshing*. Tetrahedral elements are recognized as the most suitable for meshing and adaptive remeshing but, in order to avoid numerical locking, a mixed formulation must be used in term of displacement increment Δu (or velocity v) and pressure p. Neglecting inertia forces for an elastic plastic material, for any virtual displacement Δu^* and pressure p^*, we get:

$$\int_{\Omega} (\sigma' + \Delta\sigma') : \Delta\varepsilon^* dV - \int_{\Omega} p div(\Delta u^*) dV + \int_{\partial\Omega_c} \tau_f \Delta u^* dS = 0 \quad (13)$$

$$\int_{\Omega} \left(-div(\Delta u) - \frac{\Delta p}{\kappa} + 3\alpha\Delta T\right) p^* dV = 0 \quad (14)$$

Where κ is the compressibility coefficient and α is the linear dilatation coefficient. The pressure and temperature fields are discretized using tetrahedral elements with linear shape functions N_n, and a bubble function N_b is added to the displacement field (or the velocity field), in order to stabilize the solution for incompressible or quasi incompressible materials. Introducing the nodal increment of displacement ΔU, the pressure increment ΔP and the temperature increment ΔT, we obtain a system of non-linear equations in the form:

$$R^U(\Delta U, \Delta P, \Delta T) = 0 \quad (15)$$

$$R^P(\Delta U, \Delta P, \Delta T) = 0 \quad (16)$$

$$R^T(\Delta U, \Delta P, \Delta T) = 0 \quad (17)$$

3.2. Time discretization

We have seen that the classical formulation is based on a first order time integration scheme with the displacement and pressure increment. An implicit second order scheme based on a velocity approach was proposed for a viscoplastic behavior by Bohatier and Chenot (1985) and extended to elastic plastic materials by Chenot (1984). Another approach was developed by Mole et al. (1996) in which the quasi static integral equation is differentiated with respect to time. A linear equation is obtained, which is easily solved in term of the acceleration nodal vector and velocity and displacements are given by usual time integration method. A simpler approach is to introduce an explicit Runge and Kutta integration scheme as it is presented in Traore et al. (2001) for improvement of the accuracy in ring rolling, where the number of time increments must be very large.

3.3. Space-time finite element

The space-time finite element method has received a noticeable attention since 1969, in various fields including elastodynamics, where the boundary of the domain is subjected to small deformations. But there are few contributions in the field of metal forming which exhibits large or very large deformations. The potential advantage of space-time finite elements is the possibility of a variable time increment, depending on the space location, as it is illustrated in figure 1.

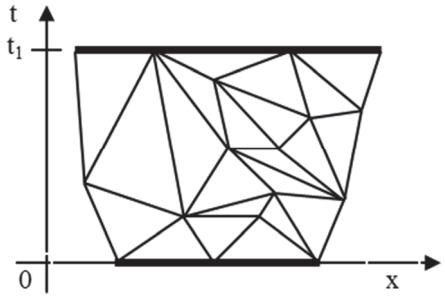

Fig. 1. *Space time discretization for a simple 1-D problem.*

Moreover error estimation can be extended to space-time in order to refine the mesh adaptively not only in locations where elements are distorted with a uniform time increment, but also to generate more elements in the time dimension with fast evolution. This approach would involve a number of numerical developments, especially for meshing and remeshing 4-dimensional domain in space and time.

3.4. Remeshing and adaptive remeshing

For a more reliable control of accuracy, an estimation of the finite element discretization error is performed and the elements must be refined locally in the zones where the strain is higher. This is achieved by prescribing a local size of the elements and imposing that the mesh is rebuilt accordingly (Fourment & Chenot, 1994).

3.5. Anisotropic remeshing

Instead of utilizing regular tetrahedra and generate a very large number of elements we prefer to

build anisotropic meshes having narrow elements in the direction of high strain gradient and elongated in the orthogonal direction (Gruau & Coupez, 2005). For that purpose a local metric matrix is defined in the local principal axes according to:

$$M = \begin{bmatrix} 1/h_1^2 & 0 & 0 \\ 0 & 1/h_2^2 & 0 \\ 0 & 0 & 1/h_3^2 \end{bmatrix} \quad (18)$$

Where h_1, h_2, h_3 are the thicknesses in the directions of principal axis of the tetrahedra to be generated locally. In practice the metric tensor is composed of several contributions. First the element should be refined in the direction of maximum gradient of the function, for example according to the strain rate tensor, we obtain the first contribution M^e to the metric. Second, when thin parts are considered a "skin adaptation" is introduced in order to define the size h_s of the mesh in the thickness; the corresponding metric is:

$$M^s = \frac{1}{h_s^2} n \otimes n \rightarrow \begin{bmatrix} 1/h_s^2 & 0 & 0 \\ 0 & 0 & 0 \\ 0 & 0 & 0 \end{bmatrix} \text{ axis } n,\ t_1, t_2 \quad (19)$$

Where n is the normal to the surface and t_1, t_2 are any orthogonal tangential unit vectors.

the radii R_1 and R_2, a new contribution to the metric is given by:

$$M^c = \frac{1}{\alpha^2} \begin{bmatrix} 0 & 0 & 0 \\ 0 & 1/R_1^2 & 0 \\ 0 & 0 & 1/R_2^2 \end{bmatrix} \text{ axis } n,\ t_1, t_2 \quad (20)$$

The α coefficient is chosen in order to impose a minimum condition of angle variation on an element. Finally the metric tensor is the sum of the three previous contributions:

$$M = M^e + M^s + M^c \quad (21)$$

In order to generate an anisotropic mesh, a similar methods is used as for the isotropic previous isotropic remeshing procedure, but the distances are evaluated with the local metric tensor. This procedure can be applied to a large variety of processes. In figure 2 a simulation of rolling is made with an anisotropic mesh of 8 786 nodes which gives the same accuracy as the computation with an isotropic computation involving 61 474 nodes.

4. RESOLUTION PROCEDURES

4.1. Linearization of the equations

The set of non-linear mechanical equations can be linearized using the classical Newton-Raphson method. We put $z = (\Delta u, \Delta p)$ and $R(z) = 0$ for the two

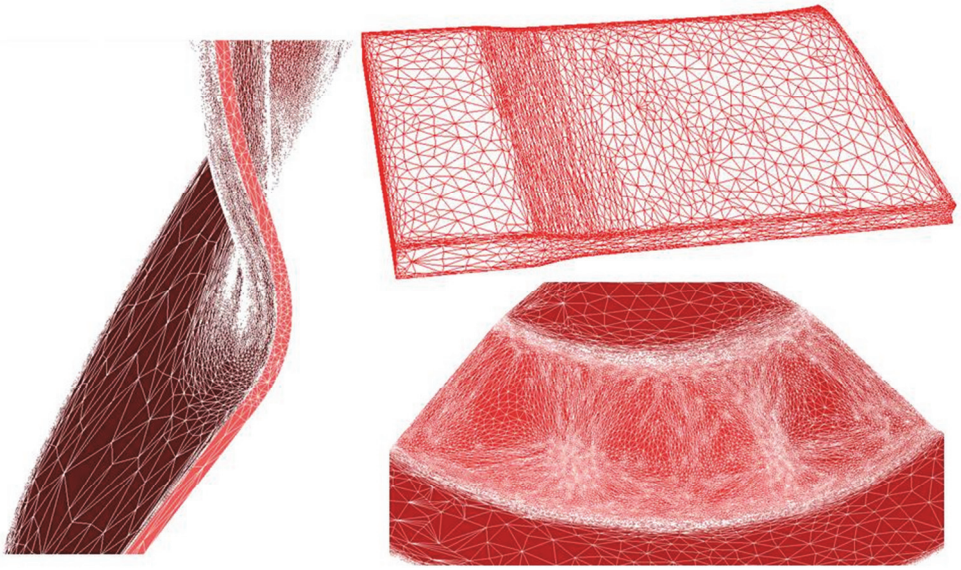

Fig. 2. *Examples of anisotropic mesh generation.*

Third, in order to take into account local curvature of the boundary of the part, which is defined by equations (15) and (16). Starting from a guess solution z^0 an iterative scheme is used to find the solu-

tion. At step number n, an increment δz^n to the current solution z^{n-1} is soughed so that $R(z^n) = R(z^{n-1} + \delta z^n) = 0$. After differentiation it is rewritten with the approximate form for computation of δz^n:

$$R(z^{n-1}) + \frac{\partial R(z^{n-1})}{\partial z}\delta z^n = 0 \qquad (22)$$

We observe that we have to solve a series of linear systems for each time increment. This process can be shortened by optimization of the residual in the direction of δz^n, which means that we minimize with respect to α the norm of the residual:

$$\left\| R(z^{n-1} + \alpha \delta z^n) \right\|^2 \qquad (23)$$

When complex constitutive laws are involved, a modified Newton-Raphson method can be used. In this case the evaluation of the derivatives of the residual can be greatly simplified by numerical differentiation, but at the expense of extra computations.

4.2. Localized contact with the tools

Tools are considered as rigid, and their surfaces are discretized by triangular facets. The signed distance δM between any point M of the domain and the tool is positive if the point is outside the tool, equal to zero if it is on the tool surface, and negative if it has penetrated into the tool. A nodal contact approach (node-to-facet) is followed. For any node n, the contact condition is prescribed at the end of the time increment:

$$0 \le \delta\left(M_n^{t+\Delta t}\right) \qquad (24)$$

This equation is linearized with the assumption that the tool can be approximated locally by its tangential plane, which will be later referred to as an explicit scheme:

$$\delta_n^{t+\Delta t} = \delta(M_n^{t+\Delta t}) \approx \delta(M_n^t) + \frac{d\delta}{dt}\left(M_n^t\right)\Delta t + O\left(\Delta t^2\right) \approx$$

$$\delta_n^{t+\Delta t} = \delta(M_n^{t+\Delta t}) \approx \delta(M_n^t) + \frac{d\delta}{dt}\left(M_n^t\right)\Delta t + O\left(\Delta t^2\right) \approx$$

$$\delta_n^t + \left(v_{tool}^t - V_n^t\right).n_n^t \Delta t \qquad (25)$$

Where v_{tool}^t is the tool velocity and n_n^t is the surface normal vector at the point of the tool surface which is the closest to node n. Contact equation (25) is enforced by a penalty formulation, which comes down at each time step t to minimizing a contact potential of the form:

$$\varphi_{contact}(V) = \frac{1}{2}\rho \sum_{n \in \partial\Omega_c} \left[\left(V_n - v_{tool}\right).n_n - \left(\frac{\delta_n + \delta_{pen}^-}{\Delta t} \right) \right]^{+2} S_n \qquad (26)$$

where ρ is a penalty coefficient, S_n is a surface portion associated to node n and δ_{pen}^- is a small numerical coefficient. This explicit formulation is accurate enough for many forming processes, but it sometimes results into numerical oscillations with important stresses or unjustified loss of contact with coarse meshes and an implicit algorithm has then to be preferred (Mahajan et al., 1998; Fourment et al., 1999). The local plane approximation of the contact surface is updated at each new Newton-Raphson iteration, rather than at the end of time increment. It allows us to take into account possible evolutions of this surface during the time step Δt. The contact condition is then written as :

$$\delta_i^{t+\Delta t} \approx \delta_{i-1}^{t+\Delta t} - \Delta v_i^{t+\Delta t}.n_{i-1}^{t+\Delta t}\Delta t \qquad (27)$$

Where i is the i[th] Newton-Raphson iteration, $\Delta v_i^{t+\Delta t}$ is the Newton-Raphson velocity correction at iteration i, $n_{i-1}^{t+\Delta t}$ the normal of the tool surface at the projection of current node $x_{i-1}^{t+\Delta t}$, that is updated as follows:

$$x_i^{t+\Delta t} = x^t + v_i^{t+\Delta t}\Delta t = x_{i-1}^t + \Delta v_i^{t+\Delta t}\Delta t \qquad (28)$$

Contact algorithm can be improved by an approach based on higher order quadratic interpolation of the tools surface (Nagata, 2005) combined with a normal voting strategy (Page et al., 2002). The resulting 3D contact algorithm provides smoother contact constraints along the discretized obstacle and increases simulation accuracy, especially in the case of metal forming processes with reduced contact area. With an explicit contact scheme, the additional computational cost is only few percent of the total computational time. With an implicit contact scheme, the continuity of the normal vectors also improves the algorithm convergence and consequently decreases its computational time.

4.3. Parallel computing

The power of computing is increasing rapidly, doubling every 18 months. It is anticipated, that in 2020, the supercomputers will have a performance

of around 1 EFlops while desktop systems will obtain a performance of up to 100 TFlops. This context imposes also significant changes on our codes and the development of fully parallel platforms to take advantage of such increases in computer processing power (Coupez et al., 2000; Mesri et al., 2008). We propose in our work an effective parallel methodology combined with mesh adaptation. Although the question of mesh adaptation has been addressed in the previous sections 3.4 and 3.5, we intend to retackle it, taking into account the current evolution of the parallel architecture, and the increase of computer powers, especially in terms of number of cores per processor.

Large scale parallel simulations involve meshes with millions to billions elements. With the increase of the latter, an interesting enhancement would be to deal with the mesh generation and adaptation in parallel. The parallelism of the mesh generator is performed here by partitioning/repartitioning the initial mesh into sub-meshes that are subsequently refined/unrefined according to the computed metric by using sequential procedure. The interfaces between subdomains remain unchanged during the local remeshing step, but are then moved along the domain to enable the remeshing in the following phases (figure 3). In other words, a repartitioning phase is performed to get unmeshed parts, those that were not yet processed, aggregated into the existing sub-domains. This partitioning/repartitioning of a mesh is performed in parallel using a generic graph partitioning that has been customized for FEM methods.

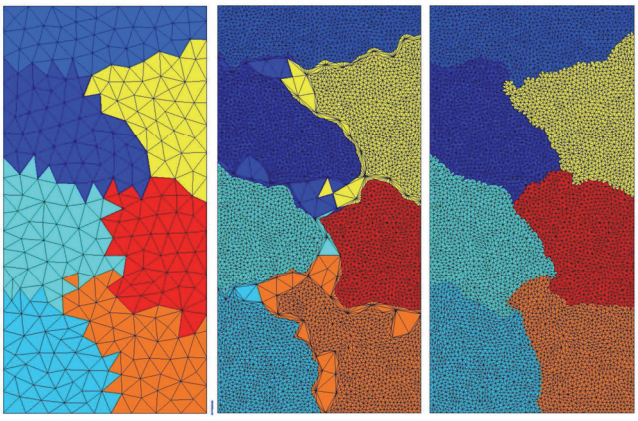

Fig. 3. *Illustration of the parallelism strategy using a 2d test case on 7 processors (from left to right)*

The proposed strategy of parallelization leads to several iterations (depending of the space dimension) between the mesher and the repartitioner, but the work to be done at each iteration decreases quickly. Indeed, an optimization method, based on a permute-copy-past algorithm, reduces the complexity from N (the data size) to m (the moving size) with m << N. It simply avoids having heavy copies of the entire data, instead it will apply permutations to the areas that need to be updated, perform the needed processing on these areas and then paste the processes area back to where they belong. This optimization was essential to obtain a costless strategy with a high parallel pay-off of the mesher.

Finally, the parallel efficiency was tested using a soft scalability test from 8 to 8192 cores. Table 1 shows the results for the resolution of the incompressible Stokes equations using a mixed P1+/P1 finite element formulation. The loading of each core is around 420000 mesh nodes (representing 1260000 unknowns per core). The results in table 1 show an almost constant time for solving the linear system that confirms the linear complexity of the algorithm but also a quasi-optimal use of all the cores as well as the memory. For thousands of cores, we have noticed an increase in the resolution time, but this is due to the strict imposed convergence rate on the coarse level grid (10^{-7}). The global system, contains more than 10 billion nodes, is solved using 8192 cores with 8 levels multigrid in 148 seconds consuming a total of 17,5Po of memory.

Table 1. *Soft scalability test case using 8 to 8192 cores on GENCI (Grand Equipement National de Calcul Intensif)*

# cores	Assembling	Resolutions	# Iterations	Memory (GB)
8	9.732	90.71	13	1.938
32	9.608	82.97	12	1.951
128	9.761	91.32	13	1.955
512	9.967	86.53	12	2.000
2048	10.60	93.7	12	2.077
8192	11.00	148.1	11	2.142

4.4. The bi-mesh method

Incremental forging simulations are still challenging due to the required number of time steps to properly describe the process. As the deformation is often confined in a localized area, the temptation is to use specific mesh boxes to refine the mesh only in such area and use coarse meshes elsewhere to speed up the simulation. But, with such a technique, when the deformation area moves and the mesh is coarsened, most of the benefit of using a fine mesh is lost as the stress/strain distribution has to be remapped from a fine grid to a coarse one. Even without dras-

tic coarsening it generates unacceptable diffusion due to cumulated remapping errors.

The first application of the bi-mesh technique was introduced by Kim et al. (1990) for ring rolling, and more recently for cogging by Hirt et al. (2007), or with a parallel implementation by Ramadan et al. (2009). The main idea is to separate the mesh devoted to the mechanical computation, called mechanical mesh (MM) in the following, from the mesh devoted to the thermal computation and to the storage of the results, called thermal mesh (TM). The user inputs a homogeneous fine thermal mesh and the software automatically derives an adapted mechanical mesh by systematic coarsening where it is allowed. The mechanical solution is computed on the adapted mesh and extrapolated on the fine mesh. As no deformation takes place in the de-refined area, extrapolation of the solution does not create any significant error. From this solution, regular updating marching scheme algorithm may be applied to update mesh geometry and associated results (strain, stress, etc.) as well. Since the thermal problem is non-local, thermal equations are solved on the fine mesh.

We summarize in figure 4 (a), the main steps of the bi-mesh algorithm. As we can see the standard single mesh algorithm (marked with white background) has been only slightly enriched by few specific steps (marked with a grey background).

The approach can be easily generalized as a multi-mesh method when more than 2 fields necessitate different mesh refinement, for example when the equivalent strain is stored in addition the velocity and temperature. An example of incremental deep drawing simulation is given in figure 5.

4.5. Remapping

Transferring data between meshes is often a necessity in metal forming applications, as for instance in the bi-mesh approach and in the ALE (Arbitrary Lagrangian or Eulerian) formulation where this operation is involved at each time step, or in the Lagragian formulation where it is appealed to at each remeshing step. The precision of this operator is obviously a key issue for the overall accuracy of the finite element method, which so requires a special attention.

In general, transferred fields can be split into two categories: primary unknowns of the problems such as velocity, pressure and temperature, and state variables such as the equivalent strain, strain rate and stresses. Firsts are usually continuous while seconds are computed at Gauss integration points and are discontinuous. With a P1+P1 velocity / pressure interpolation, they respectively are P1 (linear) and P0 (piecewise per element). Transferring data be-

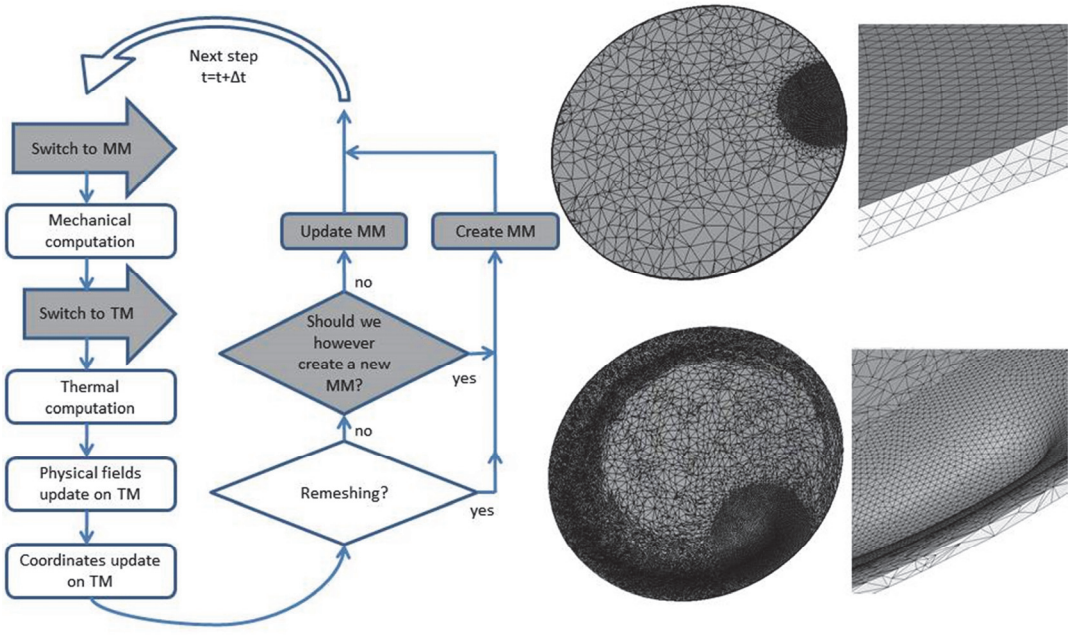

Fig. 4. *The bi-mesh algorithm. (a) General description only the steps in grey background are specific to the bi-mesh method; (b) Examples of derived mechanical meshes from a homogeneous thermal mesh.*

tween non matching meshes involves diffusion error; it is all the more important than the field is discontinuous. It is so foremost important to develop high order operators for P0 variables but as they can be appealed to at each time increment, they should be inexpensive. The key idea of the developed approach is in two steps: computing a continuous high order (P1) interpolation of state variables on the original mesh and then projecting it on the Gauss point of the new mesh. Inherent diffusion of projection is compensated by higher order of the recovered field that is derived from super convergent properties of the finite element method at Gauss points.

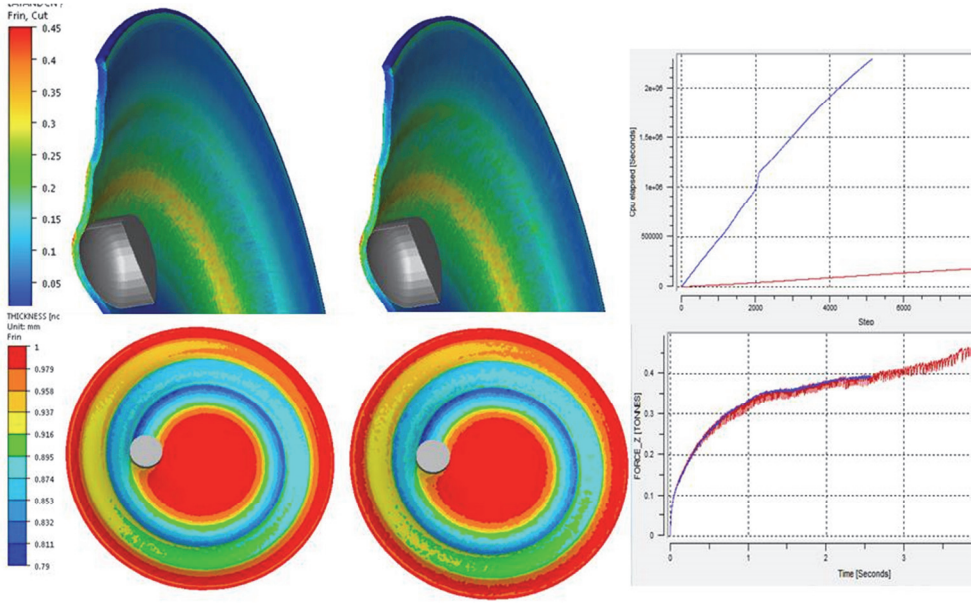

(a) (b) (c)

Fig. 5. *Incremental deep drawing forming. Latham & Cockroft criterion (up) and thickness (down). (a) With bi-mesh method;(b) Without bi-mesh method; (c) CPU time (up), vertical force on the punch (down) with bi-mesh (red lines) and without bi-mesh (blue lines).*

This approach has initially been proposed by Zienkiewicz and Zhu (1992) within the frame of error estimation (Superconvergent Patch Recovery method - SPR) before been extended to transfer operators by Khoei and Gharehbaghi (2007). Considering finite element patches (see figure 6) a local higher order continuous solution is built from super convergent values. Its value at the patch center is then used to interpolate continuously (P1) the recovered field over the original mesh. This approach is shown to be significantly more accurate than simple local averaging or than global L^2 projection. However, it does not provide the same level of accuracy on the surface of the mesh where finite element patches are incomplete, while most important phenomena such as contact, friction and heat exchange take place on domain surface in metal forming applications. This would require enlarging the size of finite element patch (see figure 6), which necessitates a complex data structure that is often difficult to build in a parallel environment.

Kumar et al. (2015) developed an iterative algorithm, where complete volume patches are first recovered, and during next iterations, incomplete patches are enriched by new values recently computed at the nodes of the patch. Such algorithm converges within 3 to 4 iterations. For transferring complex analytical functions between non-matching 3D meshes, this operator has a second order convergence rate while the simple averaging technique is only slightly more than first order; the convergence rate of the averaging operator is much lower with the surface norm while it is almost the same with the SPR operator (figure 7). For several metal forming problems involving computation of residual stresses, the enhancements brought by this transfer operator is determinant to eliminate numerical oscillations otherwise resulting from the transfer.

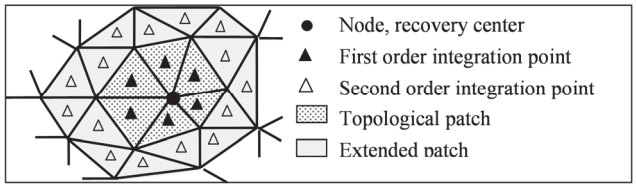

Fig. 6. *Patch centre on a node in 2D*

4.6. Multigrid

The constant need for more accuracy and reliability of computations results in smarter spatial discretizations and use of powerful parallel computers. Reducing the mesh size by a factor of 2 in each space direction results into an increase of the number of nodes by 8 (in 3D) and of the number of time increments by a factor 2. Because more than 75% of computational time of large implicit resolutions is spent during the resolution of linear systems, which computational cost is proportional to $N^{3/2}$ (N being the number of degrees of freedom), this increase in accuracy results into an increase of computational time by about 40. In order to handle larger and finer metal forming problems, it is then necessary to reduce the computational cost and more precisely the dependency of iterative solvers to the number of degrees of freedom, while keeping their parallel efficiency. According to Brandt (2002), the Multigrid method (summarized in figure 8), which has originally been developed for fluid problems, has the unique potential of providing a linear computational cost with respect to N.

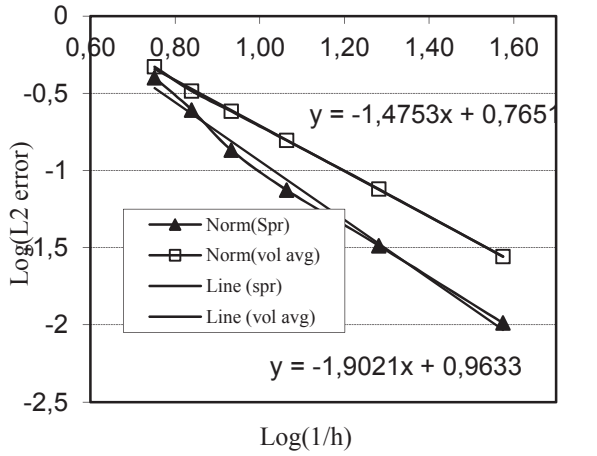

[a] Volumetric L_2 norm.

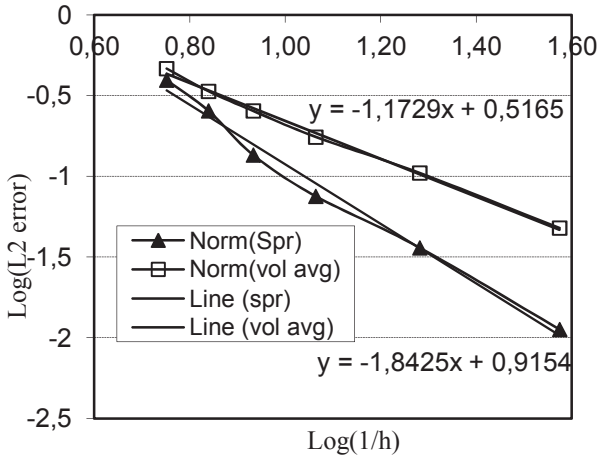

[b] Surface L_2 norm.

Fig. 7. *Comparison between SPR and Average recovery operator for the function* $f(x,y,z)=|z|(y-\beta|y|)\sin(\alpha x)$

Function $MG(A_i, r_i)$
  if $i < n$ then
    $X_i \leftarrow S(A_i, b_i)$ // pre-smoothing step
    $r_i = b_i - A_i X_i$ // residual computation
    $r_{i+1} = R_i r_i$ // residual restriction
    $\delta X_{i+1} = MG(A_{i+1}, r_{i+1})$ // correction computation
    $\delta X_i = R_i^T \delta X_{i+1}$ // correction prolongation
    $X_i \leftarrow X_i + \delta X_i$ // correction
    $X_i \leftarrow S(A_i, b_i)$ // post-smoothing step
  else
    $X_i \leftarrow D(A_i, b_i)$ // coarsest grid direct resolution
  return X_i
end

Fig. 8. *Multigrid V-cycle algorithm*

For metal forming applications, obtaining such property requires using several special features for the choice of the smoothers (the linear solvers that are used at each level of the multi-level algorithm), for the construction of coarse levels using a Galerkin

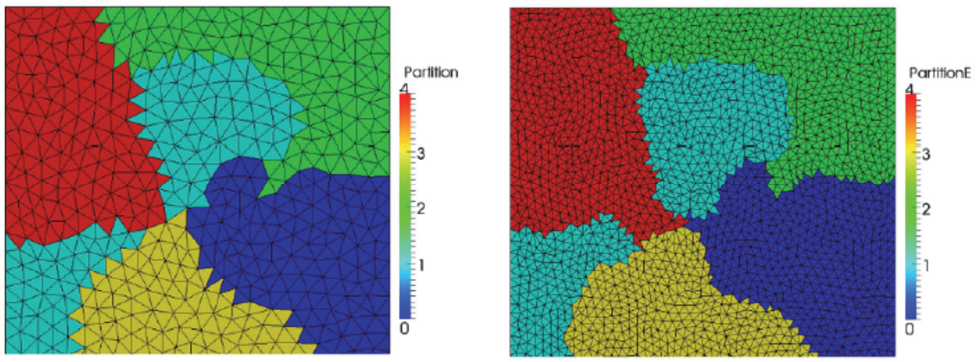

Fig. 9. *Parallel partitioning of a square where different colors refer to different processors. Right: fine mesh. Left: coarse mesh built in parallel from fine mesh.*

/ algebraic approach rather than a geometrical approach, and for the automatic building of the coarse meshes (from finer unstructured meshes of very complex shapes as encountered in material forming): see Rey et al. (2008). An additional issue regards the compatibility with parallel computations, which consequently requires carrying out all these operations in parallel, and more particularly the construction of coarse meshes (see figure 9) and the transfer between the meshes.

An application of the multigrid method to a representative forging problem is shown in figure 10. It is computed on a 12 processors machine where the multigrid solvers exhibits the same parallel efficiency as original Krylov solver.

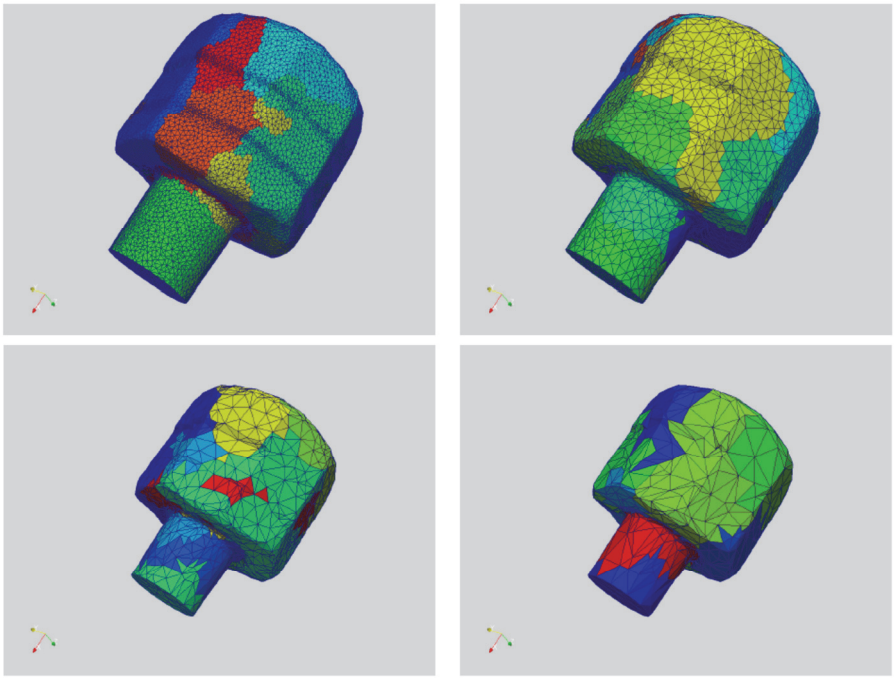

Fig. 10. *A four levels multigrid method partitioned onto 12 processors for forging simulation. Finer mesh of 87 00 nodes (top left), intermediate meshes of 11 900 nodes (top right), 3 800 nodes (bottom left) and 1 670 nodes (bottom right).*

5. COUPLED APPROACHES

5.1. Thermal and mechanical coupling

At this stage, several methods can be used, depending on the thermal and mechanical coupling. When coupling is weak enough, the mechanical and thermal problems are solved separately and the coupling is postponed to the next increment. For intermediate coupling a separate resolution is still used, but fixed point iterations are performed. For strong coupling and strain rate localization, the global system is solved by a Newton-Raphson method on V, P, and T (or ΔU, ΔP and ΔT) as reported in Delalondre (2008).

5.2. Multi material coupling and self contact

Let us first consider a two bodies problem with, discretized domains Ω_a and Ω_b their contact between their interfaces $\partial\Omega_a$ and $\partial\Omega_b$ corresponding to separate meshes. For point M located on $\partial\Omega_a$, with normal n_a, we define δ_{ab} as the distance to $\partial\Omega_b$ along n_a. Non-penetration is defined by: $\delta_{ab} \leq 0$. Similarly, h_{ba} is the distance along the normal vector n_b from $\partial\Omega_b$ of any point to $\partial\Omega_a$. The contact constraint can be treated numerically by the penalty method with a normal contact force (in a similar way as described in section 4.2). In the symmetric formulation, the following penalty contributions are added to Eq. (4), for any virtual velocity fields v_a^* and v_b^*:

$$-\rho \int_{\partial\Omega_a} h'_{ab} n_a v_a^* \mathrm{d}S - \rho \int_{\partial\Omega_b} h'_{ba} n_b v_b^* \mathrm{d}S \qquad (29)$$

The symmetric method was proposed by Habraken and Cescotto (1998) for structural computation, involving small displacements. But for material forming, where large relative displacements generally occur, this method introduces many numerical constraints and results in a too stiff interface.

In the "Master and Slave" approximation originally proposed by Hallquist et al. (1985), we impose only that the "Slave" surface $\partial\Omega_a$ must not penetrate the "Master" surface $\partial\Omega_b$. For any virtual velocity field v_a^*:

$$-\rho \int_{\partial\Omega_a} h'_{ab} n_a v_a^* \mathrm{d}S \qquad (30)$$

The "Master and Slave" approximation, is preferred as it permits satisfactory computation of the boundary. We observe that numerical results are satisfactory provided that the mesh of the slave surface $\partial\Omega_a$ is more refined than that of master surface $\partial\Omega_b$ and a reduced integration method is introduced to avoid over constrained contact condition.

In the "Quasi symmetrical method" a compromise is found between the symmetric formulation and the Master and Slave method, replacing Eq. (9) by the following terms:

$$-\rho \int_{\partial\Omega_a} h'_{ab} n_a v_a^* \mathrm{d}S - \rho \int_{\partial\Omega_b} h'_{ba} n_b \pi_{ab}(v_a^*) \mathrm{d}S \qquad (31)$$

Where $\pi_{ab}(v_a^*)$ is the projection of v_a on the boundary $\partial\Omega_b$.

This approach was first proposed by Fourment (2008) with a slightly different formulation.

These approaches were compared with the "Single mesh method" in Chenot et al. (2014), on extrusion coating and bending of a tube composed of 4 materials.

Self contact events can be viewed as a special case of contact between deformable bodies, and be treated with a master-slave algorithm. Fictitious elements, that link a node on the master body to a facet on the slave body, are geometrically built and used to integrate the contact equations. For more details on these numercial techniques the interested reader can refer to (Fourment et al., 1999; Chenot et al., 2002; Fourment et al., 2004).

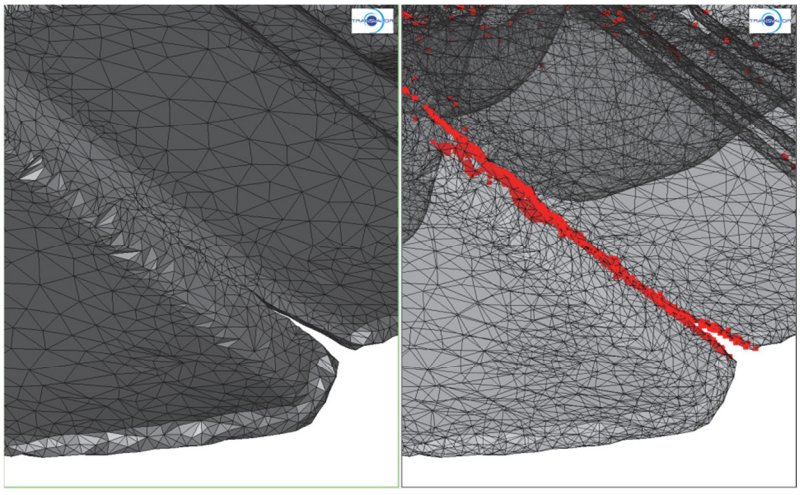

Fig. 11. *Simulation of material folding.*

In the case of self-contact events, the numerous remeshing that are performed during the simulation might results in an important smoothing of the fold surfaces. Since the accurate localization of the defaults due to folding surfaces in the final part is of high importance, self-contact is combined with a particle algorithm to trace the folds surface during the whole computation. Each time a node is found inside an element, that is not located in its immediate vicinity, a fold particle is created and followed until the end of the simulation. Such an algorithm results in the creation of a large number of particles that allow us to describe accurately these surfaces (see figure 11).

5.3. Electromagnetic heating

Induction heating is a process widely used to heat a billet, or a preform, before hot forming or heat treatment. Generally heating of the work-piece does not provide a uniform temperature distribution, the accurate knowledge of the temperature distribution is necessary for the numerical simulation of the following deformation process and microstructure evolutions.

In order to compute the temperature increase in the work-piece the electromagnetic phenomena must be modeled and coupled with thermal simulation. We utilize the simplified set of Maxwell equations obtained after physical approximations corresponding to induction heating usual conditions.

$$div\left(\frac{1}{\rho^{el}} div(V^{el})\right) = 0 \qquad (32)$$

$$\frac{1}{\rho^{el}}\frac{\partial A}{\partial t}+curl\left(\frac{1}{\mu^{m}}curl(A)\right)=\frac{1}{\rho^{el}}grad(V^{el}) \tag{33}$$

Where A is the vector of magnetic potential, V^{el} is the scalar of electric potential, ρ^{el} is the electrical resistivity and μ^{m} is the magnetic permeability. Note that to ensure uniqueness of the solution, we assume:

$$div(A)=0 \tag{34}$$

The electric potential equation (32) can be put into a weak integral form; for any scalar test function φ:

$$\int_{\Omega}\frac{1}{\rho^{el}}grad(V^{el}).grad(\varphi)dV-\int_{\partial\Omega_2}j^{s}.n\varphi dS=0 \tag{35}$$

$\partial\Omega_2$ is the surface of the inductor where the vector of electric current density j^s is applied, and $V = 0$ is imposed on the opposite surface of the inductor.

Utilizing linear tetrahedral elements, the potential field is discretized and the corresponding approximation of equation (35) is solved in term of nodal values of the electric potential.

For the magnetic potential A, the integral form of eq. (33) takes the following form for any test vector ψ:

$$\int_{\Omega}\frac{1}{\rho^{el}}\frac{\partial A}{\partial t}.\psi dV+\int_{\Omega}\frac{1}{\mu^{em}}curl(A).curl(\psi)dV=\int_{\Omega}j.\psi dV \tag{36}$$

The electric current is evaluated with:

$$j=\sigma^{el}grad(V^{el}) \tag{37}$$

Where we have introduced the resistivity σ^{el}.

Following Nédélec (1986), we have utilized special elements, where the magnetic potential is defined on the edges of the tetrahedra. The coupling condition with the heat equation imposes to add a source term to take into account the electromagnetic heating. It is introduced by its average over a period of the alternating current in the inductors.

We have:

$$E=-\frac{\partial A}{\partial t}-grad(V) \tag{38}$$

In the part we assume:

$$grad(V)=0 \tag{39}$$

The source term is averaged according to:

$$Q_{em}=\frac{1}{T^{f}}\int_{0}^{T}\sigma\|E\|^{2}=\frac{1}{T^{f}}\int_{0}^{T}\sigma\left\|\frac{\partial\mathbf{A}}{\partial t}\right\|^{2} \tag{40}$$

All of the physical parameters depending on temperature and magnetic field are updated at each time step.

For more computational details, the interested reader may refer to Bossavit (1993) and Cardinaux (2008).

An example of application of induction heating to a rotating ring is illustrated in figure 12. Other applications can be found in Cardinaux et al. (2010).

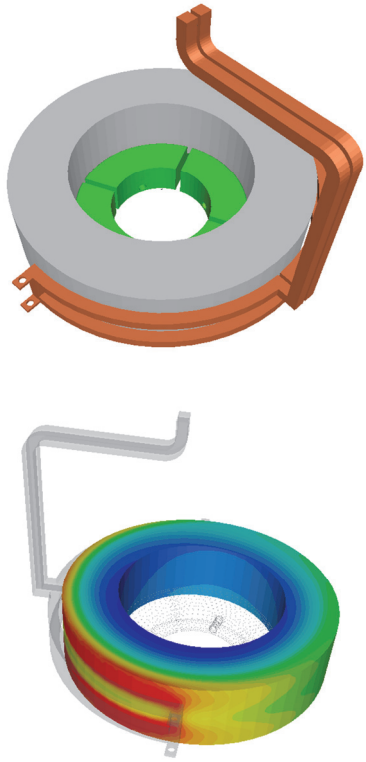

Fig. 12. *Induction heating of a ring. Up: schematic view of the inductor and the ring. Down: temperature distribution (maximum in red is about 550°C).*

5.4. Heating in industrial furnaces

5.4.1. Introduction

In materials science, the simulation of transient heat transfer characteristics of the steel in an industrial furnace or in a water quenching bath is still the subject of considerable amount of research investigations especially with the increasing demands for lowering energy consumption and pollutant emissions (see e.g. Song et al. (1997)). Recall that the

heating process represents a critical step to achieve the correct temperature and metallurgical properties of the treated work-pieces. We can clearly identify many factors that play an important role in such processes: minimization of local temperature gradients, ensuring a uniform temperature within the load, avoiding at maximum all surface defects such as skid marks, controlling the cooling rate (quenching velocity), minimizing energy usage, maximizing the furnace capacity and the quality of the steel product in terms of hardness, toughness and resistance.

However, the complex three-dimensional structure of a furnace or a quenching bath, including the thermal coupling of fluids and solids, the turbulent convection, the thermal radiation, the location of the treated work-pieces, the orientation of the burners, the quenching fluid, and the given geometry, make the problem difficult to analyze accurately and economically. Therefore, the design of a computational fluid dynamics (CFD) tool is valuable for the exploration and the prediction of these physical phenomena.

In order to solve the above mentioned issues, our work focuses on developing a direct coupled approach capable of handling and simulating these phenomena that take place in a complex 3D configuration. In particular, it focuses on accurately representing the physical domains (gas and solid in the present case), and dealing with the conjugate heat transfer that occurs among them. The main steps are the following.

First, an Immersed Volume Method (IVM) is applied to perform the multidomain computation (fluid/solid). It uses a single global mesh in which the different domains are taken into account by the use of the level set function. Consequently, only one set of equations with different thermal properties is solved. This avoids the use of empirical data to determine any heat transfer coefficients at the fluid-solid interface. The heat exchange is replaced naturally by solving the Navier-Stokes equations in the whole domain.

Second, the stabilized finite element methods were adjusted to account for fluid solid interactions. Emphasis has been given to deal with the convection dominated regimes when solving the heat transfer equation and the k-epsilon turbulence model. A particular attention has been given to treat numerically the thermal shocks that occur right after the sudden heating of a solid. It consists in using the standard enriched finite element approaches with time-interpolation. It is applied to the transient conduction heat equation where the classical Galerkin method is shown to be unstable. It adds and eliminates bubbles by static condensation to the finite element space and then interpolates the solution to the real time step. These modifications are equivalent to the addition of stabilizing terms tuned by a local time-dependent stability parameter, which ensures an oscillating-free solution.

Finally, the boundary condition for radiative heat transfer is replaced by solving an additional radiative transport equation (RTE) in both domains using the so-called P-1 model. This will generate a volume source term that is in turn introduced into the energy equation and rendered by the sharp discontinuity of the temperature and the material properties.

5.4.2. Immersed Volume Method

The Immersed Volume Method is an interesting tool for computational engineers, in particular for conjugate heat transfer analysis. It can be easily implemented in finite element codes. It allows solving a single set of equations for the whole computational domain and treating different subdomains as a single fluid with variable material properties. This offers a great flexibility to deal with different shapes or to change easily the physical properties for each immersed structure. Therefore, we start by computing the signed distance function of a given geometry to each node in the mesh. Using the zero isovalue of this function, we can easily identify the fluid-solid interface. Consequently, we can apply an anisotropic mesh adaptation at this interface and then mix the thermo-physical properties appropriately for both domains. In what follows, we recall briefly all the needed step.

Level set and distance functions

At any point x of the computational domain , the level set function α corresponds to the signed distance from Γ_{im}. In turn, the interface Γ_{im} is given by the zero isovalue of the function α:

$$\alpha(x) = \pm d(x, \Gamma_{im}), x \in \Omega,$$
$$\Gamma_{im} = \{x, \alpha(x) = 0\} \quad (41)$$

We use the following sign convention: $\alpha \geq 0$ inside the solid domain defined by the interface Γ_{im} and $\alpha \leq 0$ outside this domain. As explained, the signed distance function is used to localize the interface of the immersed structure, but it is also used to initialize the desirable properties on both sides of the

interface. Indeed, for the elements crossed by the level set functions, fluid-solid mixtures are used to determine the element effective properties. The Heaviside function can be smoothed to obtain a better continuity at the interface using the following expression:

$$H_\varepsilon(\alpha)=\begin{cases}1 & \text{if } \alpha>\varepsilon\\ 0.5(1+\alpha/\varepsilon+1/\pi\sin(\pi\alpha/\varepsilon) & \text{if } |\alpha|\le\varepsilon\\ 0 & \text{if } \alpha<-\varepsilon\end{cases} \tag{42}$$

where ε is a small parameter such that ε = O(h_{im}), known as the interface thickness, and h_{im} is the mesh size in the normal direction to the interface. In the vicinity of the interface, it can be computed using the following expression:

$$h_{im}=\max_{j,l\in K}\left(grad(\alpha).(x_l-x_j)\right) \tag{43}$$

where K is the set of node indices of the mesh element under consideration. According to the chosen formulation, the Heaviside function is then approximated using linear interpolations (P1) between fluid and solid properties or a piecewise constant interpolation (P0).

Level set and anisotropic mesh adaptation

We combine next the level set representation with an anisotropic mesh adaptation algorithm to ensure an accurate capturing of the discontinuities at the fluid-solid interface. The level set function intersects the mesh element arbitrarily. It is possible then to overtake the discontinuity appearing at the interface by using anisotropic mesh adaptation and regularization. The regularization parameter can be seen as the thickness or the resolution of the interface. It is shown that using local adaptivity, stretched elements at the interface are obtained enabling a very small resolution of the thickness and leading to very sharp interfaces, favorable for simulating fluid-structure interactions and conjugate heat transfer.

This anisotropic adaptation is performed by constructing a metric map that allows the mesh size to be imposed in the direction of the distance function gradients. Moreover, we can prescribe a default mesh size, or background mesh size, h_d far from the interface and reduce it as the interface comes closer. A likely choice for the mesh size evolution is the following:

$$h=\begin{cases}h_d & \text{if } |\alpha(x)|>\varepsilon/2\\ \dfrac{2h_d(m-1)}{m\varepsilon}|\alpha(x)|+\dfrac{h_d}{m} & \text{if } |\alpha(x)|\le\varepsilon/2\end{cases} \tag{44}$$

Eventually, at the interface, the mesh size is reduced by a factor m with respect to the default value h_d. Then this size increases gradually to reach h_d for a distance that corresponds to the half of a given thickness ε. The above defined unit normal to the interface x and the mesh size h, leads to the following metric:

$$M=C(x\otimes x)+\frac{1}{h_d}I \quad \text{with}$$

$$C=\begin{cases}0 & \text{if } |\alpha(x)|\ge\varepsilon/2\\ \dfrac{1}{h^2}-\dfrac{1}{h_d^2} & \text{if } |\alpha(x)|<\varepsilon/2\end{cases} \tag{45}$$

where I is the identity tensor. This metric corresponds to an isotropic metric far from the interface (with a mesh size equal to h_d for all directions) and to an anisotropic metric near the interface (with a mesh size equal to h in the x direction, and equal to h_d in the other directions).

Level set and mixing laws

Once the mesh is well adapted at the interface, the material distribution among the domains can be described by means of the level set function. Consequently, the same set of equations: the momentum equations, the energy equation, the turbulent kinetic and energy equations, and the radiative transport equations are simultaneously solved over the entire domain with variable material properties. The use of the smoothed Heaviside function regularizes and enables the assignment of the right properties on each side of the interface. The material properties such as density, viscosity as well as the initial temperature, heat capacity and mean absorption coefficient, are computed as follows:

$$\begin{aligned}\rho&=\rho_f H(\alpha)+\rho_s(1-H(\alpha))\\ \mu&=\mu_f H(\alpha)+\mu_s(1-H(\alpha))\end{aligned} \tag{46}$$

However, as far as the thermal conductivity is concerned, linear interpolation would lead to inaccurate results. According to Hachem (2013), one has to resort to the following law to ensure the conservation of the heat flux:

$$\lambda = \left(\frac{H(\alpha)}{\lambda_f} + \frac{1-H(\alpha)}{\lambda_s} \right)^{-1} \qquad (47)$$

5.4.3. Stabilized Finite element methods

We are interested in simulating the coupled heat transfer and fluid flow problem using the Reynolds-Averaged Navier-Stokes equations including the Boussinesq approximation and the k-ε model. Therefore, one has to solve the following coupled non-linear system in Ω:

$$\begin{aligned} & grad(v) = 0 \\ & \rho\left(\frac{\partial v}{\partial t} + v.grad(v)\right) - div(2\eta_e \dot{\varepsilon} - p_e I) = \rho_0 \beta (T - T_0) g \\ & \rho C_p \left(\frac{\partial T}{\partial t} + v.grad(T)\right) - div(\lambda_e grad(T)) = f - grad(q_r) \end{aligned} \qquad (48)$$

where v is the velocity vector, p_e the effective pressure, T the temperature, ρ the density, η is the dynamic viscosity, $\dot{\varepsilon}$ the strain rate tensor , ρ_0 and T_0 are respectively the reference density and temperature, β is the thermal expansion coefficient and g is the gravitational acceleration. Eventually, the third equation denotes the energy conservation and it involves the constant pressure heat capacity C_p, the specific effective thermal conductivity λ_e, a volume source term f and the heat radiative flux q_r. Note that for sake of simplicity, we kept the same notation for the averaged values of the unknowns such as the velocity v, the effective pressure p_e and the temperature T. This system features also the effective viscosity η_e and the effective thermal conduction λ_e which are given by:

$$\eta_e = \eta + \eta_t \text{ and } \lambda_e = \lambda + \frac{C_p \eta_t}{P_{r_t}} \qquad (49)$$

with P_{r_t} = 0.85 the turbulent Prandtl number. The turbulent viscosity η_t in expression is a function of the turbulent kinetic energy k and the turbulent dissipation ε, that reads:

$$\eta_t = \rho C_\eta \frac{k^2}{\varepsilon} \qquad (50)$$

with C_η is an empirical constant usually equal to 0.09. The introduced variables k and ε are computed using the two-equations turbulence model that reads:

$$\begin{aligned} & \rho\left(\frac{\partial k}{\partial t} + v.grad(k)\right) - div\left(\left(\eta + \frac{\eta_t}{P_{r_k}}\right) grad(k) \right) = \\ & \qquad P_k - P_b - \rho\varepsilon \\ & \rho\left(\frac{\partial \varepsilon}{\partial t} + v.grad(\varepsilon)\right) - div\left(\left(\eta + \frac{\eta_t}{P_{r\varepsilon}}\right) grad(\varepsilon) \right) = \\ & \qquad \frac{\varepsilon}{k}\left(C_{1\varepsilon} P_k + C_{3\varepsilon} P_b - C_{2\varepsilon} \rho\varepsilon\right) \end{aligned} \qquad (51)$$

Here P_k represents the production of turbulent kinetic energy due to the mean velocity gradients, P_b is the production due to the buoyancy effects, Pr_k and Pr_ε are the turbulent Prandtl number for k and ε respectively, while $C_{1\varepsilon}$, $C_{2\varepsilon}$ and $C_{3\varepsilon}$ are model constants (Launder and Spalding, 1974). The production terms P_k and P_b are modelled as follows:

$$P_k = 2\eta_t \dot{\varepsilon} : \dot{\varepsilon} \text{ and } P_b = -\frac{\eta_t}{\rho P_{r_g}} g\, grad(\rho) \qquad (52)$$

Indeed, these last equations can be represented by a scalar transient convection-diffusion-reaction type of equation which reads:

$$\frac{\partial \varphi}{\partial t} + v.grad(\varphi) + div\left(\alpha grad(\varphi)\right) + r\varphi = f \qquad (53)$$

where φ is the scalar variable, v the velocity vector, α the diffusion coefficient, r the reaction coefficient and f a source term. The solution strategy for solving such an equation is similar to that used for the equations of motion. Thus, the Galerkin formulation is obtained by multiplying these equations by appropriate test functions, applying the divergence theorem to the diffusion terms and integrating over the domain of interest. Following the lines on the use of stabilization methods for transient convection-diffusion- reaction equations, as discussed in Codina et al. (2008), the stabilized weak form can be written according to equation 54. Find a scalar function φ such that for any test function w:

$$\begin{aligned} & \int_\Omega \Big(\left(\frac{\partial \varphi}{\partial t} + v.grad(\varphi)\right) w + \left(\alpha grad(\varphi).grad(w)\right) + \\ & r\varphi w - fw \Big) dV + \sum_K \int_{\Omega_K} \left(\left(R(\varphi) \tau_{SUPG}\, v.grad(w) \right) dV \right. \\ & \left. + \sum_K \int_{\Omega_K} \left(\left(R(\varphi) \tau_{SCPG}\, \tilde{v}.grad(w) \right) dV = f \right. \end{aligned} \qquad (54)$$

where $R(\varphi)$ is the appropriate residual, v is the convection velocity and $\tilde{v}$ is an auxiliary vector function of the temperature gradient. Two additional

stabilizing terms have been introduced; the first one, denoted SUPG, controls the oscillations in the direction of the streamlines (Brooks & Hughes, 1982) and the second one, denoted SCPG, controls the derivatives in the direction of the solution gradient (Galeao & Do Carmo, 1988). This can improve the result for convection dominated problems while the shock-capturing technique precludes the presence of overshoots and undershoots by increasing the amount of numerical dissipation in the neighborhood of layers and sharp gradients. The evaluation of the τ_{SUPG} and τ_{SCPG} stabilizations terms follows the definitions described in (Galeao & Do Carmo, 1988). A general theta-scheme was implemented for the time discretization of these equations with an implicit backward-Euler time-integration scheme ($\theta = 1$).

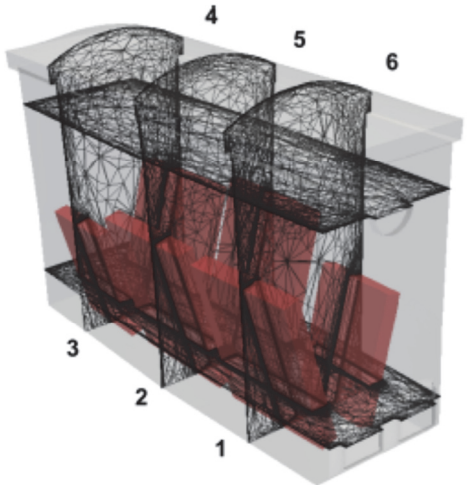

Fig. 13. *Computational domain after anisotropic mesh adaptation.*

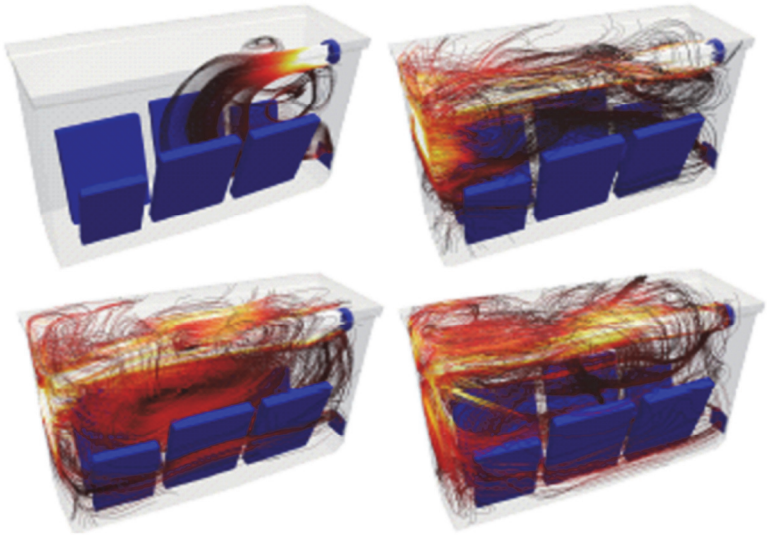

Fig. 14. *Streamlines distribution inside the furnace and around the ingots.*

5.4.4. Industrial application

In this section, we present briefly 12 hours of heating inside an industrial furnace provided by our industrial partner Industeel Arcelor Mittal. Figure 13 shows six ingots taken initially at 400°C and positioned at different locations inside the furnace and table 2 summarizes the main physical data. The hot gas is pumped into the furnace through one burner located on the vertical wall having a constant speed of 38m/s and a temperature of 1350°C. The final mesh used for the numerical simulation consists of 157, 347 nodes and 884, 941 tetrahedral elements. An adaptive time-step is used starting from 0.001s and increases as the solution stabilizes.

Table 2. *Material properties*

Properties	Gas	Steel 40CDVL3
Density ρ (kg/m^3)	1.25	7,800
Heat capacity C_p (J/kg/°K)	1000	600
Viscosity μ (kg/m/s)	1.9 10^{-5}	-
Conductivity λ (W/m/°K)	0.0262	37
Emissivity ε	-	0.87

The 3D computations have been obtained through two steps using 128 cores (2.4 Ghz Opteron) in parallel, and was completed after about one day of computational time using space-time adaptivity. Figure 14 illustrates the gas motion in the furnace around the ingots.

Figure 15 shows the temperature distribution on four mutual planes in the furnace for two different time steps, allowing the user to predict phase changes during the heating process.

5.5. Physical coupling with micro structure evolution

Three approaches, working at different length scales, are used to predict the microstructural evolution during forming processes.

The classical semi-empirical JMAK approach is based on the global description of the recrystallized fraction in constant conditions of strain rate and temperature. Recrystallization kinetics (implying nucleation of new grains, their growth and the impingement of the growing grains) are described by the analytical Johnson-Mehl-Avrami-Kolmogorov (JMAK) equation.

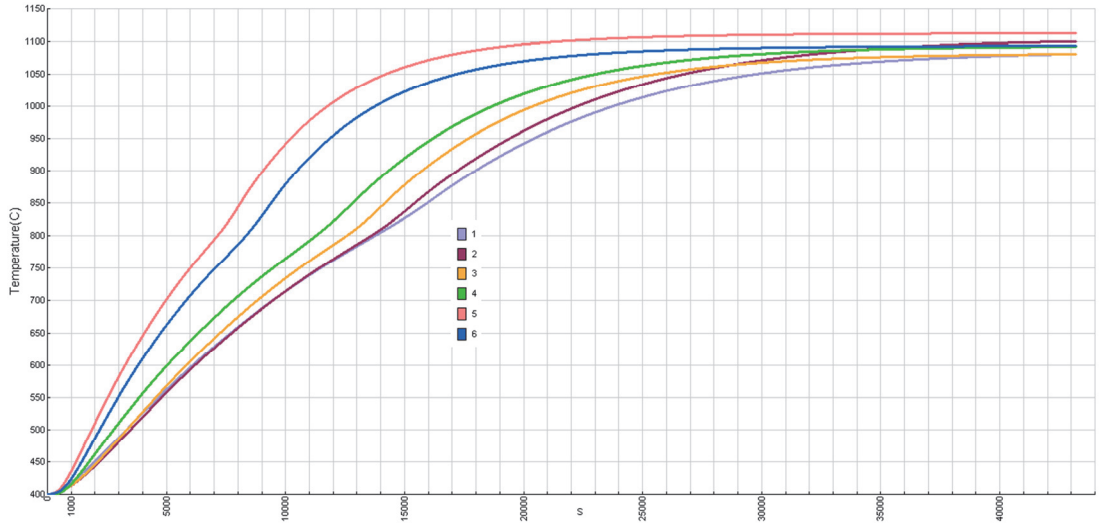

Fig. 15. *Temperature-time profile captured at the center of the immersed ingots.*

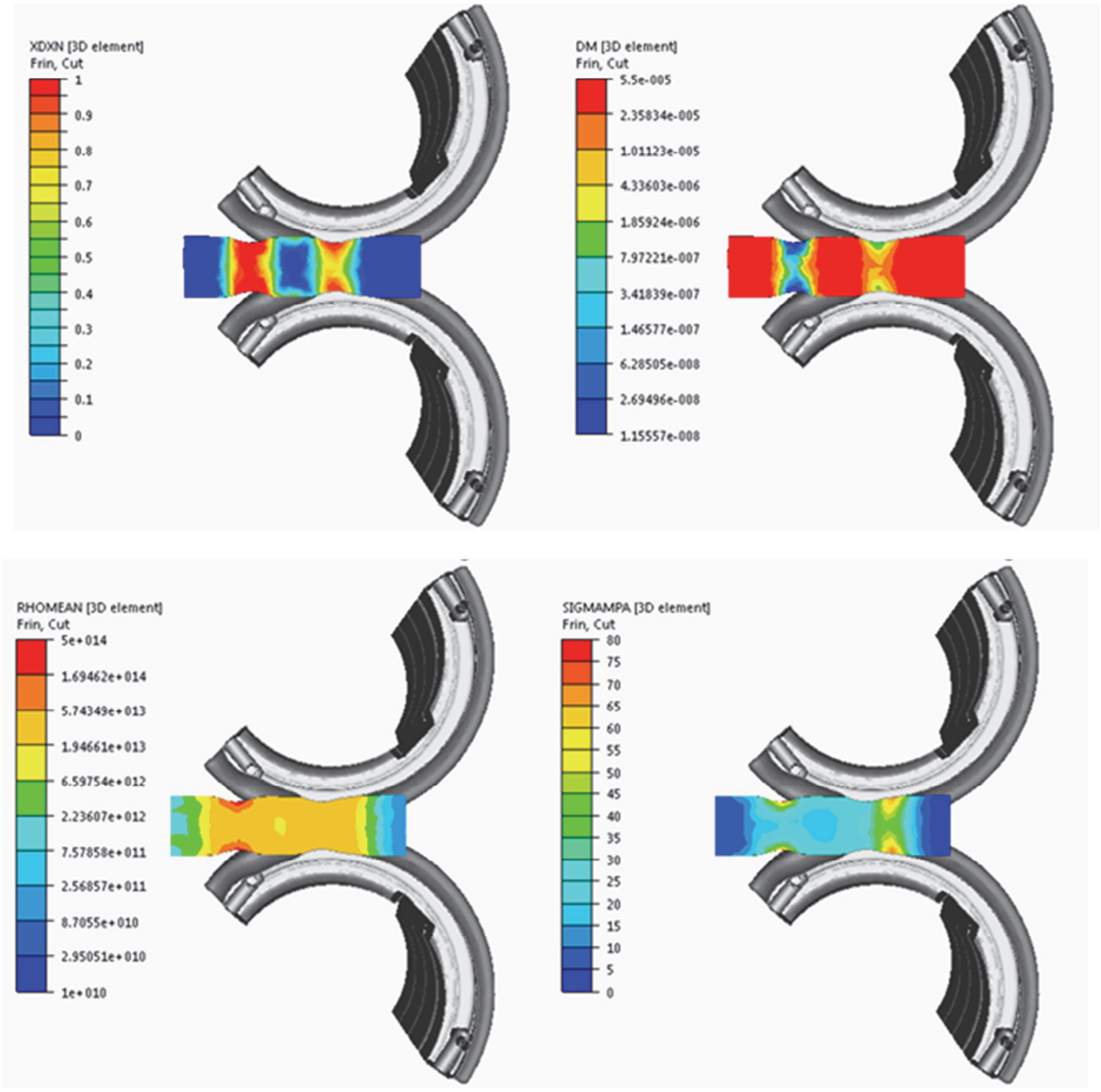

Fig. 16. *Reducer-rolling simulation coupled with the mean-field model for microstructure evolution. Upper left: recrystallization ratio; Upper right: grain size; Lower left: mean dislocation density; Lower right: yield stress*

$$X(t) = 1 - e^{-b.t^n} \tag{55}$$

Where X is the recrystallized fraction and b and n the Avrami's coefficients obtained by fitting the experimental curves. Dynamic, post-dynamic and static recrystallization can be considered; the different recrystallized fractions and diameters depend on the process parameters (strain, strain rate and temperature) and initial grain size. Implemented in the FORGE® software, the model has undergone several modifications in order to be used with any thermo-mechanical local loading and to take into account multiple recrystallization steps that can be encountered during multi-pass processes see Teodorescu et al., 2007.

The mean-field approach was developed in the general context of multi-pass metal processing. It uses equations based on the physics of strain-hardening, recovery, grain boundary migration, nucleation and precipitation. Input parameters have a physical meaning (e.g. Burgers vector, shear modulus, grain boundary mobility, etc.). The microstructure is described by a set of internal variables representative of the material (average dislocation densities and grain sizes). According to Mukherjee et al. (2010) and Bernard et al. (2011), the microstructural evolution is directly given by the evolution of these parameters during the forming process.

Since the metal behavior depends on the dislocation density, such approach allows a direct coupling with the rheological behavior of the material. CPU times associated with these methods are generally low, making them suitable for coupled calculations and allowing simulations at each integration points of a finite element mesh (figure 16).

The evolution of the dislocation density is given by:

$$\frac{d\rho_d}{dt} = A_0 + A_1 \cdot \sqrt{\rho_d} - A_2 \cdot \rho_d - A_2 \cdot \rho_d^{5/2} - A_4 \cdot \rho_d^{5/2} \cdot Arg\,sinh\left(\frac{A_5}{\sqrt{\rho_d}}\right) \tag{56}$$

Where A_1, A_2, A_3, A_4, A_5 are material parameters, identified by comparison with experimental data. The mean dislocation density is expressed according to:

$$\rho_m = \rho_d \cdot (1 - X) + \rho_x \cdot X \tag{57}$$

Where X is the percentage of recrystallization and ρ_x the dislocation density in the recrystallized fraction. Finally the local yield stress can be computed:

$$\sigma = M \cdot \alpha_p \cdot b \cdot \mu \cdot \sqrt{\rho_m} + \frac{M \cdot K_b \cdot T \cdot \sqrt{\rho_m}}{c_9 \cdot b^2} \cdot Arg\,sinh\left(\frac{A_5}{\sqrt{\rho_m}}\right) \tag{58}$$

with the help of the additional physical parameters: M, α_b, b, μ, K_b and $c9$.

The full-field method is discussed in section 7.

6. OPTIMIZATION AND IDENTIFICATION

6.1. Process optimization

Optimization is often the actual purpose of numerical simulation. In metal forming, it usually involves a small number of parameters which can be quite complex as they often regard 3D tool shapes. Consequently, great efforts have been dedicated to the coupling of optimization algorithms with CAD tools, as shown in figure 17 where the parameters of the CAD representation of a preform shape are directly linked to the optimization algorithm.

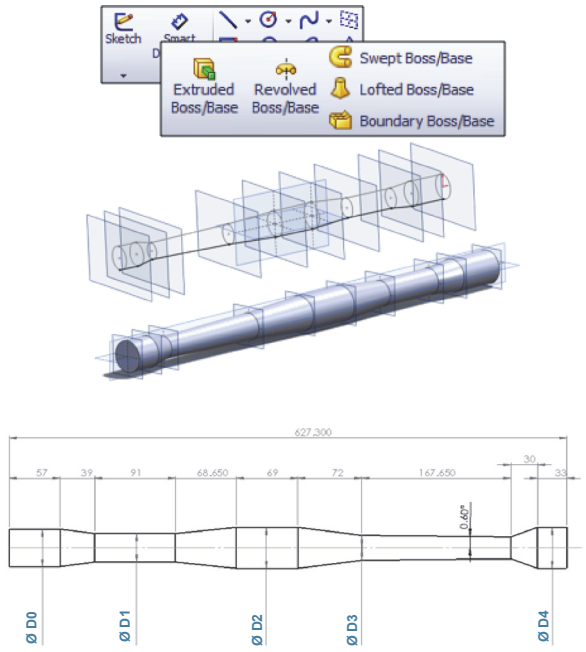

Fig. 17. CAD parameterization (left) of the preform shape of a three-stepped forged car component and its 4 optimization parameters (right).

Other features of metal forming problems regards the computational time of simulations and the complexity of the optimization problem, which can either be very small with almost linear problems or very high with many local extrema and uncertainties, resulting either from numerical noise (in particular due to remeshing and data transfer) or from the

process model itself (friction, lubrication, material models …). All these features plead toward using robust but expensive algorithms, such as evolutionary algorithms, combined with metamodeling which allows reducing computational cost. A key point for the accuracy and efficiency of such metamodel based algorithm consists in dynamically improving the metamodel with new computations during the convergence of the optimization algorithm see Bonte et al. (2010). In this context, numerical noise can be handled by filtering the very high frequencies of objective functions through the smoothing of the metamodel as presented in figure 18. We observe that for a wire drawing problem, a straightforward variation of the maximum drawing force with respect to the die angle and die length shows an unphysical extremum due to numerical noise due to remeshing (with coarse meshes), while smoothing allows removing this biased solution. Metamodel-based evolution algorithms can easily be extended to multi-objective optimization problems, in order to handle the full complexity of most engineering problems with several objectives and constraints. In this frame, there is not a single optimum but a Pareto surface of possible compromises

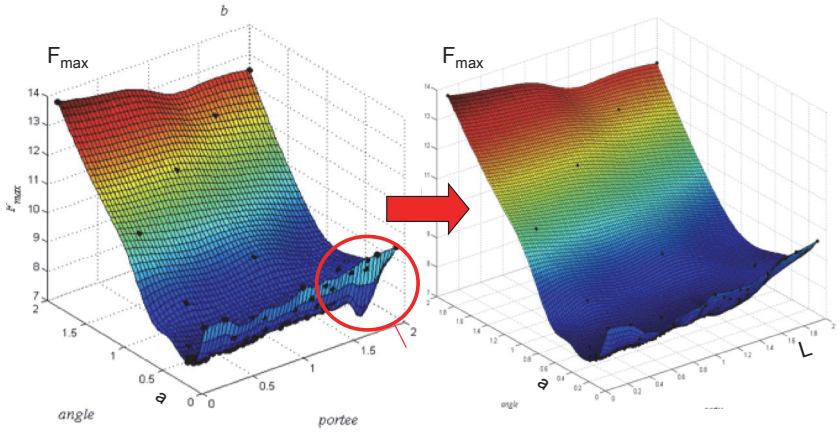

Fig. 18. Left: metamodel of the noisy objective function exhibiting an unphysical extremum. Right: smoothed metamodel with no unphysical extremum.

The computational cost of optimization is consequently increased by the need to enlarge the domain of accuracy of the metamodel as shown by Edjay and Fourment (2010). This additional cost is often justified by the quality of provided information and new understanding about the forming process.

6.2. Identification of material parameters

Identifying correctly material parameters is essential if one wants to get accurate results with any kind of material behavior law and damage model. Identification strategies using inverse analysis are now widely used when dealing with complex non-linear behaviors. The main idea of inverse approaches is to fit numerical results coming from a FE simulation on experimental data. This fitting is done iteratively by tuning the material parameters values in the model in order to minimize a cost function. This cost function is based on the gap between numerical and experimental observables. The choice of these observables and their number is important if one wants to avoid any parameters correlation or non-unique solutions issues (Roux, 2011). This is particularly true when dealing with ductile damage due to the competition between hardening on the one hand and softening (coming both from necking and damage growth) on the other hand. The use of local observables in addition to global observables (such as the classical load-displacement curve) is a good way of enriching the cost function. Local observables may be based on necking measurements (Roux & Bouchard, 2011) or full displacement field measurements (Roux, 2011). Enhancing the experimental basis to avoid non-unique solutions may also require the use of multiple experimental tests (Cao et al., 2013). Finally, some micromechanical models may require the use of microstructure observations. Regarding ductile damage parameters identification, in-situ X-Ray tomography appears to be a powerful solution. This technique enables to count the number of voids and to give their size evolution all along the mechanical test. This approach was successfully used in (Cao et al., 2014b) for the identification of a Gurson based damage model.

7. COMPUTATION AT THE MICRO-SCALE

7.1. General approach

It is well known that the micro (or nano) structure of metals is a key factor for determining the constitutive law during forming and for predicting the final properties of the work-piece. To treat in an average way, the evolution of the material microstructure during thermal and mechanical treatments, the classical method, well known as “mean field

approach", consists in fact in a macro description, selecting representative material parameters (grain size, inclusions, phase percentage, precipitates, etc.) and to identify physical laws which govern the evolution of these parameters, and their influence on the mechanical behavior. The macro approach is quite convenient for coupling thermal, mechanical and physical computation, but it suffers severe limitations and needs a large amount of experiments to identify the physical laws describing microstructure evolution. It is so obvious that these models must be calibrated and improved by models which take into account explicitly the topological and physical features of the microstructure. Moreover computation at the microscale is now possible and is developed for a potentially more realistic description of materials under the concept of "full field approach". Micro modeling is potentially much more accurate but, due to heavier computer cost at the local micro level, direct coupling with macro thermal and mechanical simulations seems limited to 2D problems and simple parts, even with large clusters of computers. If, as already detailed, one interest of these developments is to use the micro approach to help identification and improvement of mean field models; another way to view the short term applications is to use micro modeling of material in post processing, to predict micro structure evolution for a limited number of locations in the work piece, neglecting coupling effects.

These challenges explain firstly the development, over the last twenty years, of new numerical methods to generate digital materials at a microscopic or mesoscopic scale, which would be statistically or exactly equivalent to the considered microstructure in terms of topology and attributes and the concept of Representative Element Volume (REV) (Dawson, 2000; Dawson et al., 2005; Brahme et al., 2006; Xu & Li, 2009; Bernacki et al., 2009; Hitti et al., 2013; Saby et al., 2013). The generation of statistical virtual polycrystals in context of recrystallization (ReX) or of spheres dense packing in context of powder metallurgy remain fertile research domains (see figure 19). Secondly, these challenges explain the development of numerical methods dedicated to the modeling of dynamic boundary problems. Probabilistic methods associated to a voxel (or pixel in 2D) can be based on grain structure descriptions; for instance, Monte-Carlo (MC) and Cellular Automaton (CA) approaches have been successfully applied to ReX, grain growth (GG) and phase transformations (Rollett & Raabe, 2001; Wang & Liu, 2003; Kugler & Turk, 2004).

The standard MC method as derived from the Potts model (multistate Ising model) applies probabilistic rules at each cell and at each time step of the simulation. In this model, the interfaces are implicitly defined thanks to the membership of the cells to the various grains. In this context, some probabilistic evolution rules are applied to describe the boundary motion phenomena. The CA method uses physically based rules to determine the propagation rate of a transformation from one cell to a neighbouring cell, and can therefore be readily applied to the microstructure change kinetics of a real system.

Three main methods can be found in the literature for finite element calculations on virtual microstructures : the "vertex" models (VM) also called "front tracking" models, the "Phase Field" method (PFM) and the "Level Set" method (LSM). The VM is the only one to be based on an explicit description of the considered interfaces thanks to surface elements of the considered finite element mesh or grid. Historically, the VM was developed to describe the GG (Nagai et al., 1990). In these models the grain boundaries are considered as continuous interfaces transported by a velocity defined thanks to the local curvature of the grains boundaries. The main idea is to model the interfaces by a set of points and to move these points at each time increment by using the velocity and the normal to the interfaces. It explains the other name for this approach, "front tracking". Complex topological events such as the disappearance of grains or node dissociations are treated thanks to a set of rules which is completed by a repositioning of the nodes. More recently, the VM was extended in order to take into account both ReX and GG, together with site saturated nucleation (Piekos et al., 2008a). In 2D, results for isotropic GG show good agreement with the theory (Piekos et al., 2008b). It remains difficult to deal with the non-natural treatment of topological events, mainly in 3D, when the set of rules become very complex and numerically expensive (Weygand et al., 2001; Syha & Weygand, 2010).

The PFM (Chen, 1995; Militzer, 2011) and the LSM (Sethian, 1996) methods have many common points. In both approaches, an interface is described implicitly thanks to an artificial field, so that tracking interfaces as in VM is not an issue anymore. However, these two approaches require to work with high order finite elements or with very fine finite elements meshes to obtain an accurate description of

the interfaces. The artificial field is built as a continuous approximation of the Heaviside function in PFM (hence the notion of diffuse interface) whereas it corresponds to the distance function at the interface in LSM. The initial concept of the PFM was to describe the location of two phases (Collins & Levine, 1985). This concept has been extended to deal with more complex problems involving more than two phases and for modelling microstructure evolution (Chen, 2002; Karma, 2001). In the case of polycrystalline microstructures, each grain orientation is used as a non-conserved order parameter field and the free energy density of a grain is formulated as a Landau expansion in terms of the structural order parameters. The grain boundary energy is introduced as gradients of the structural order parameters and the boundaries themselves are represented by an isovalue of the order parameter fields. As for the MC or CA methods, the topological events are treated in a natural way as a result of energy minimization. Numerous publications have illustrated the potential of this approach for ideal normal GG modelling in 2D context (Chen, 2002) and more recently in 3D (Moelans et al., 2009), for static and dynamic ReX (Takaki et al., 2008) for abnormal GG (Ko et al., 2009) and for Zener Pinning phenomena (Chang et al., 2009). Discussions in the literature point out the current limitations of PFM regarding free energy density functions which can reproduce the physical properties of the material. One other problem arises for very rapid change in the phase field across the diffuse interface which can lead to very expensive and intensive calculations, particularly for three-dimensional systems.

The LSM concept is quite old (Osher & Sethian, 1988), but its application to dynamic interface problems at the microstructure scale is quite recent. First models for 2D or 3D primary recrystallization include site saturated or continuous nucleation stage as illustrated in figure 20 (Logé et al., 2008; Bernacki et al., 2008; Bernacki et al., 2009). They were applied to very simple microstructures, and then improved to be able to deal with more realistic 2D and 3D microstructures and to make the link with stored energies induced by large plastic deformations see also Resk et al. (2009).

Anisotropic meshing and remeshing techniques can be used to accurately describe interfaces, both for modelling plastic deformation using crystal plasticity, and for updating the grain boundary network at the recrystallization stage. Interestingly, it was also shown that the distribution of stored energy in a polycrystal resulting from plastic deformation led to deviations from the Johnson-Mehl-Avrami-Kolmogorov (JMAK) theory. Recently, for the modeling of ReX and GG phenomena, the LSM has been used by Elsey et al. (2009) in context of regular grid

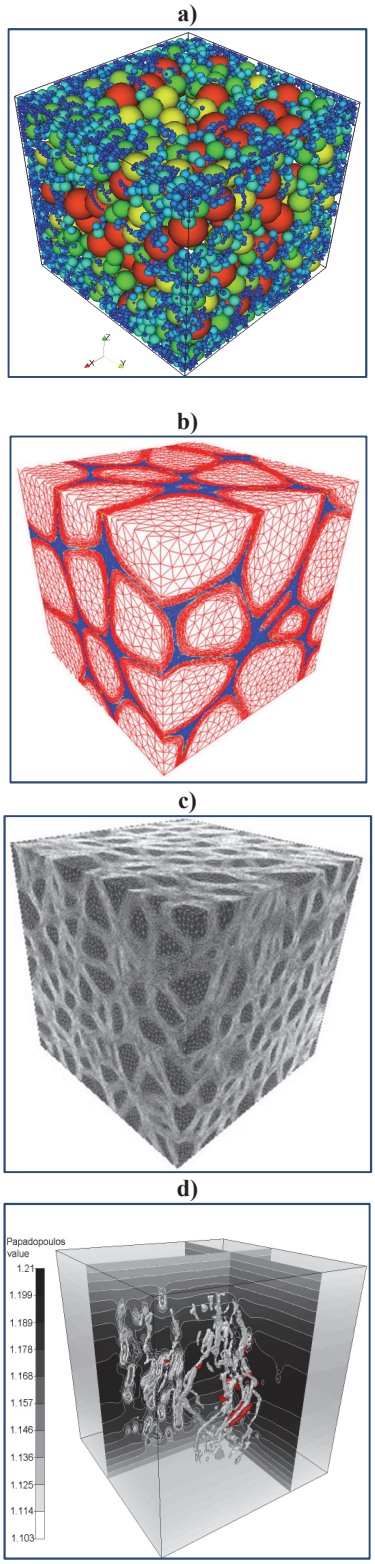

Fig. 19. *Examples of REVs respecting initial statistical data: (a) a 304L powder, (b) semi-solid granular with liquid in blue (anisotropic mesh), (c) 304L polycrystal with anisotropic finite element mesh in white, (d) a cluster of MnS particles.*

and in (Bernacki et al., 2011; Hallberg, 2013; Jin et al., 2014; Fabiano et al., 2014; Agnoli et al., 2014) in context of FE approach. It is also interesting to underline current development of the LSM in order to model ductile damage phenomena at the microscale as illustrated in figure 21 (Roux et al., 2013; Roux et al., 2014). The current main weakness of LSM remains, as in PFM, the numerical cost since very fine element meshes have to be used to track the grains interfaces, particularly in 3D.

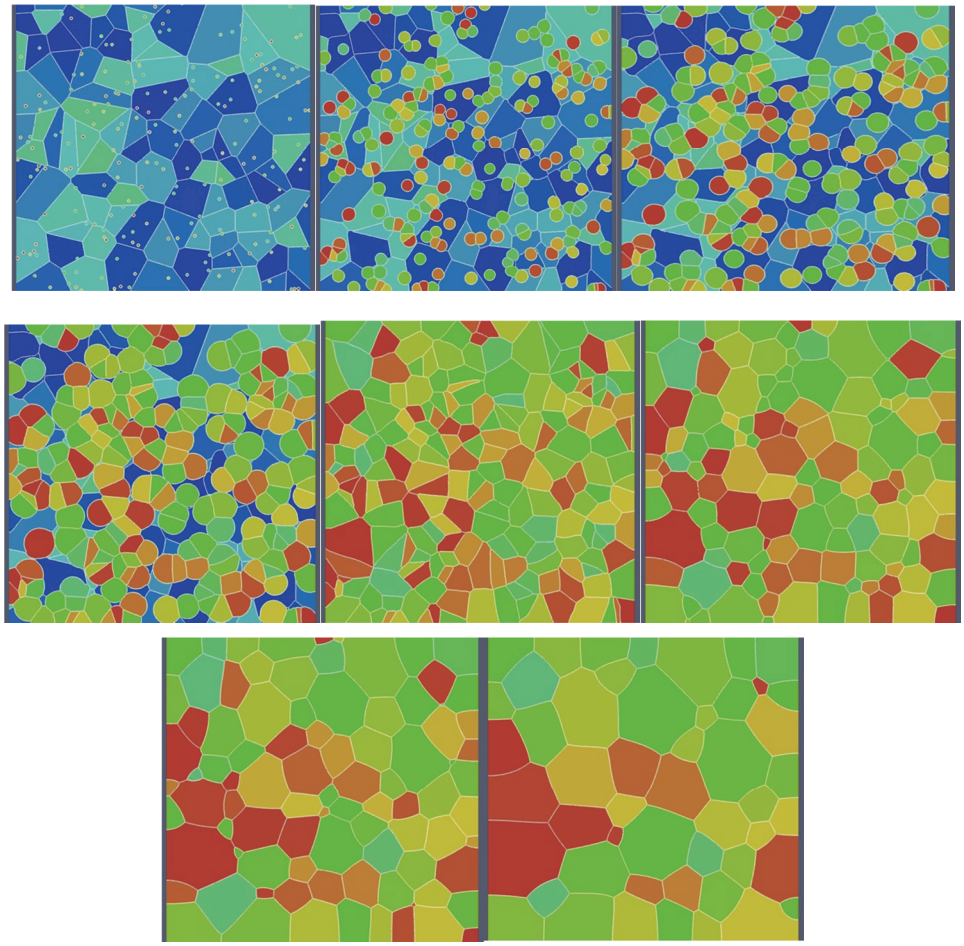

Fig. 20. *Site-saturated nucleation in 304L stainless steel, from top to bottom and left to right : modeling of primary ReX and subsequent GG modeling thanks to the LSM.*

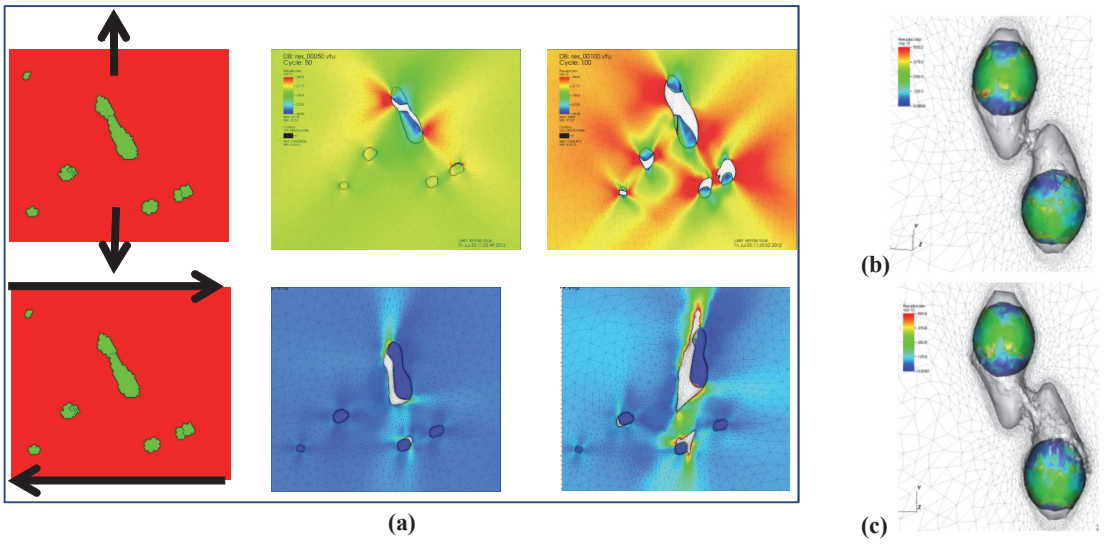

Fig. 21. *Influence of loading conditions on nucleation mechanism. a) particles fracture or debonding; b) and c) coalescence stage in tension for a 3D configuration.*

This brief description of some results could be completed by another realized developments concerning modeling of microstructural evolutions at the REV scale. In fact, all these developments converge toward the same objectives, i.e. to provide a set of numerical tools in order to improve macroscopic models thanks to simulations realized at the microscopic scale but also to provide a better understanding of very local microstructural evolutions which cannot be predicted by classical empirical mean field approaches. Moreover FE commercial software dedicated to these topics are now considered as a necessity in some industrial contexts.

7.2. Identification using finite element micro modeling

Such micro-modeling approaches are very promising regarding the understanding of plastic and damage mechanisms for complex thermo mechanical loadings as well as the calibration of mean field models.

statistical reconstruction. FE simulations on these REV with the appropriate boundary conditions are performed in order to extract microscopic evolution laws. In figure 21, void volume fraction as a function of plastic strain is plotted. These evolution laws are then used to identify mean-field damage models parameters which in the end will be used in macroscopic scale FE simulations. The same methodology is applied in (Saby et al., 2013; Saby et al., 2014) to define a suitable void closure criterion and identify its parameters.

8. FUTURE CHALLENGES:

8.1. Process stability and introduction of stochastic phenomena

Provided that the problem is well modeled, numerical simulation is predictive and describes accurately all phenomena of interest. It means that the finite element discretization error is low and often much lower than errors resulting from the modeling

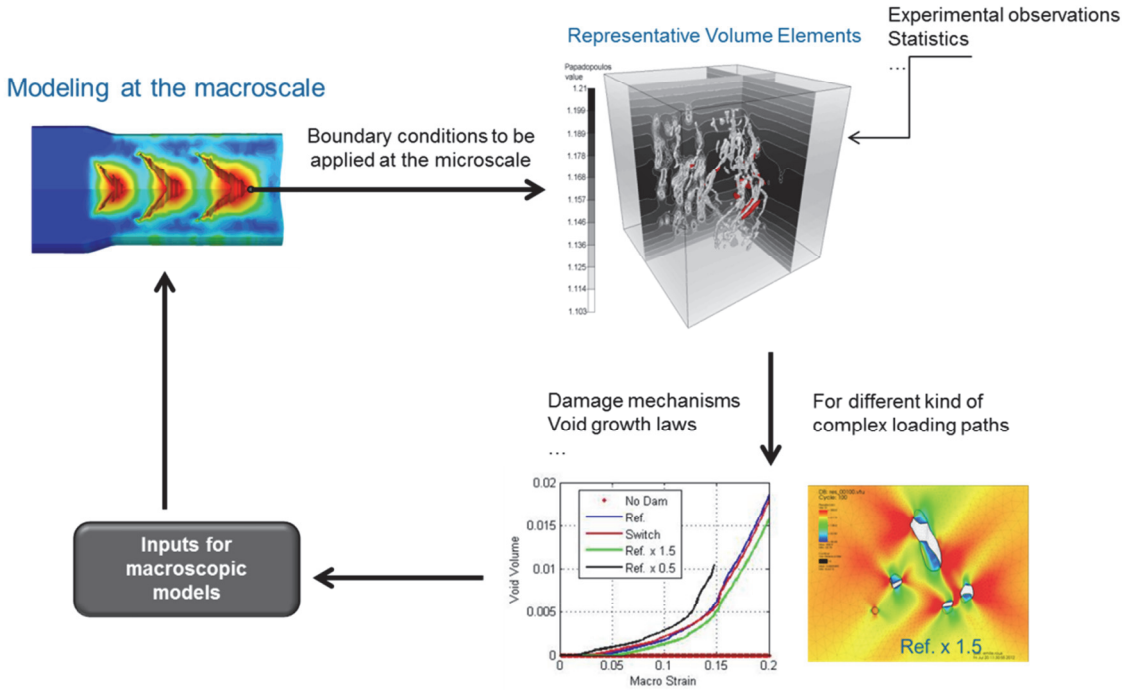

Fig. 22. Multiscale methodology to identify mean-field models parameters thanks to microscale FE simulations.

Figure 22 shows the strategy that can be applied to identify mean-field models parameters based on micromechanical modeling. Numerical sensors are placed on finite element simulations of the process at the macro scale in order to extract loading paths. This loading path can be used as boundary conditions for FE simulations at the micro-scale on representative volume elements (REV). These REV are built either from experimental observations or from

of the problem. Taking into account the main sources of these uncertainties is a major challenge of computations. Uncertainties have many origins: changes of material origin, lubrication conditions or process parameters but also approximate modeling of interface and material behavior, or else geometry description, boundary conditions, etc. The challenge consists in first identifying, modeling and quantifying these uncertainties and then in taking them into

account during process simulation and optimization (Strano, 2008). Monte-Carlo approaches are obviously too expensive while stochastic formulations show quite difficult to implement into existing software. Most promising approaches rely on advanced metamodels that can be either used for a Monte-Carlo type approach (Fourment, 2007) or extended to model the stochastic nature of the results (Zabaras et al., 2000; Lebon et al., 2014) and can be both used to render process variability and allow robust optimization (Wienbenga et al., 2013).

8.2. Model reduction

Reducing computational time remains a major challenge. New emerging techniques show quite efficient and effective: the Proper Orthogonal Decomposition (PGD) method is one of them. It allows carrying out real time simulations, provided that precomputations have been carried out in advance in a proper way (Chinesta & Cueto, 2014). In the frame of highly non-linear metal forming problems, a first step would be to extend Model Reduction Techniques resulting from Proper Orthogonal Decomposition (Ryckelynck, 2009). In some other fields such as fluid mechanics or structural mechanics, they allow reducing the computational time by several order of magnitude through a dramatic reduction of the number of unknowns, down to ten or at least less than one hundred. They are based on projections onto main problem modes, which are computed in advance from previous simulation results. It sounds reasonable to try to extend them first to simple metal forming problems.

8.3. Toward simulation of the whole processes chain

Forming process simulation started in the 70th with, as a main objective, to predict forming forces, forming defects such as under filling, folding and possible cracks. When this has been achieved, focus has started to move to the dies with the goal to predict and improve die life and reduce production costs. If there are still some progress to be done, stress distribution and die wear are now available in simulation packages. This second point being achieved, focus is back on the component with a specific attention to "in use properties". These properties are the results of the whole manufacturing chain: starting with the initial forming process (rolling, cogging or wire drawing), going through the whole chain to ends with the final heat treatments (carburizing, quenching, nitriding, tempering). Depending on the situation, some of the "in use properties" are already available by simulation while others are still ahead. Significant progresses have been made in recent years and it is now possible to simulate and to optimize complete chains of simulations (Ducloux et al., 2013). The contributions of upstream stages such as ingot casting or continuous casting can also be taken into account and then allow to monitor the complete process chain with the prediction of porosities, segregations, concentrations of chemical elements during solidification to their evolution during the phases of forging. It gives a better understanding of the internal structure of the forged part (Jaouen et al., 2014a) and for example can be an aid in the design of shells produced from hollow ring (Jaouen et al., 2014b).

For a better understanding of the "in use properties" a finer description of the micro structure is needed. It requires predicting and following the micro structure evolution through the whole process chain which is still a topic in progress and existing models still need to be developed and improved in order to optimize computation time.

9. CONCLUSIONS

After many years of continuous development, simulation of metal forming processes by the finite element method has reached an undisputable level of reliability and is currently utilized in many industrial companies for predicting important technical parameters. Most of mechanical issues are treated satisfactorily, even if computational developments are still necessary to optimize numerical treatments and take into account new problems. Now within the next 10 or 20 years lots of effort is necessary to model accurately the physical evolution of metallic materials during forming and heat treatments and to predict the final properties of work-pieces and assemblies.

REFERENCES

Agnoli, A., Bozzolo, N., Logé, R., Franchet, J.-M., Laigo, J., Bernacki, M., 2014, Development of a level set methodology to simulate grain growth in the presence of real secondary phase particles and stored energy – Application to nickel-based superalloy, *Comp. Mater. Sci.*, 89, 233-241.

Archard, J. F., Hirst, W., 1956, The Wear of Metals under Unlubricated Conditions, *Proceedings of the Royal Society*, A 236, 397-410.

Barlat, F., Lian, J., 1989, Plastic behaviour and stretchability of sheet metals (Part I) A yield function for orthotropic sheet under plane stress conditions, *Int. J. Plasticity,* 5, 51-56.

Bernacki, M., Chastel, Y., Coupez, T., Logé, R. E., 2008, Level set framework for the numerical modelling of primary recrystallization in polycrystalline materials, *Scripta Mater.,* 58, 12, 1129-1132.

Bernacki, M., Resk, H., Coupez, T., Logé, R., 2009, Finite element model of primary recrystallization in polycrystalline aggregates using a level set framework, *Simul. Mater. Sci. Eng.*, 17, 064006, doi:10.1088/0965-0393/17/6/064006.

Bernacki, M., Loge, R., Coupez, T., 2011, Level set framework for the finite-element modelling of recrystallization and grain growth in polycrystalline materials, *Scripta Mat.,* 64, 525-528.

Bernard, P., Bag, S., Huang, K., Logé, R. E., 2011, A two-site mean field model of discontinuous dynamic recrystallization, *Materials Science and Engineering*, A 528, 7357-7367.

Bohatier, C., Chenot, J.-L., 1985, Finite element formulations for non-steady-state large viscoplastic deformation, *Int. J. for Numerical Methods in Engineering*, 21, 9, 1697-1708.

Bonte, M., Fourment, L., Do, T., van den Boogaard, A., Huétink, J., 2010, Optimization of forging processes using Finite Element simulations, *Structural and Multidisciplinary Optimization,* 42, 5, 797-810.

Bossavit, A., 1993, Electromagnétisme en vue de la modélisation, *Mathématiques et applications,* 14, Springer-Verlag, Paris, France (in French).

Bouchard, P.-O., Bourgeon, L., Fayolle, S. Mocellin, K., 2011, An enhanced Lemaitre model formulation for materials processing damage computation*, Int. J. Mater. Form.,* 4(3), 299-315.

Brahme, A., Alvi, M. H., Saylor, D., Fridy, J., Rolett, A. D., 2006, 3D reconstruction of microstructure in a commercial purity aluminum, *Scripta Mater.,* 55, 1, 75-80.

Brandt, A., 2002, Multiscale Scientific Computation: Review 2001, in *Multiscale and Multi resolution Methods*, T. Barth, T. Chan, and R. Haimes Editors., Springer, Berlin, 3-95.

Brooks, A. N., Hughes, T. J. R., 1982, Streamline upwind/Petrov-Galerkin formulations for convection dominated flows with particular emphasis on the incompressible Navier-Stokes equations, *Computer Methods in Applied Mechanics and Engineering*, 32, 199-259.

Cao, T.S., Gaillac, A., Montmitonnet, P., Bouchard, P.-O., 2013, Identification methodology and comparison of phenomenological ductile damage models via hybrid numerical-experimental analysis of fracture experiments conducted on a zirconium alloy, *International Journal of Solids and Structures,* 50, 24, 3989-3999.

Cao, T.-S, Gachet, J.-M, Montmitonnet, P., Bouchard, P.-O., 2014, A Lode-dependent enhanced Lemaitre model for ductile fracture prediction at low stress triaxiality, *Engineering Fracture Mechanics*, 124-125, 80-96.

Cao, T.S., Maire, E., Verdu, C., Bobadilla, C., Lasne, P., Montmitonnet P., Bouchard P.-O., 2014b, Characterization of ductile damage for a high carbon steel using 3D X-ray micro-tomography and mechanical tests - Application to the identification of a shear modified GTN model, *Computational Materials Science*, 84, 175-187.

Cardinaux, D., 2008, Etude et modélisation numérique 3D par éléments finis d'un procédé de traitement thermique de tôles embouties après chauffage par induction : application à un renfort de pied central automobile, *PhD Thesis, Mines Paristech*, Sophia-Antipolis, France (in French).

Cardinaux, D., Bay, F., Chastel, Y., 2010, A coupled multi-physics model for induction heat treatment processes, *Computer Methods in Materials Science*, 10, 4, 307-312.

Chang, K., Feng, W., Chen, L.Q., 2009, Effect of second-phase particle morphology on grain growth kinetics, *Acta Mater*., 57, 5229-5236.

Chen, L.-Q., 1995, A novel computer simulation technique for modeling grain growth, *Scr. Metall. Mater.*, 32, 1, 115-120.

Chen, L.-Q., 2002, Phase-field models for microstructure evolution, *Ann. Rev. Mater. Res.*, 32, 113-140.

Chenot, J.-L., 1984, A velocity approach to finite element calculation of elastoplastic and viscoplastic deformation processes, *Engineering Computations*, 5, 1, 2-9.

Chenot, J.-L., Béraudo, C., Bernacki, M., Fourment, L., 2014, Finite element simulation of multi material metal forming, 11th International Conference on Technology of Plasticity, *Procedia Engineering* 10/2014; 81:2427-2432. DOI: 10.1016/j.proeng.2014.10.345.

Chenot, J.L., Fourment, L., Mocellin, K., 2002, Numerical treatment of contact and friction in FE simulation of forming processes, *J. Mater. Process. Technol.,* 125-126, 45-52.

Chinesta, F., Cueto, E., 2014, Introduction, in PGD-Based Modeling of Materials, Structures and Processes*, ESAFORM Bookseries in material forming*, Springer International Publishing, 1-24.

Codina, R., Gonzalez-Ondina, J. M., Diaz-Hernandez, G., Principe, J., 2008, Finite element approximation of the modified Boussinesq equations using a stabilized formulation, *International Journal for Numerical Methods in Fluids*, 57, 1249-1268.

Collins, J. B., Levine, H., 1985, Diffuse interface model of diffusion-limited crystal growth, *Phys. Rev. B*, 31, 9, 6119.

Cornfield, G. C., Johnson, R. H., 1973,Theoretical predictions of plastic flow in hot rolling including the effect of various temperature distributions, *J. Iron Steel Inst*., 211, 567.

Coupez T., Digonnet H., Ducloux R., 2000, Parallel meshing and remeshing, *Applied Mathematical Modelling,* 25, 153-157.

Dawson, P. R., 2000**,** Computational crystal plasticity, *Int J. Solids Struct*., 37,1-2, 115-130.

Dawson, P. R., Miller, M. P., Han, T.-S., Bernier, J.-L., 2005, An accelerated methodology for the evaluation of critical properties in polyphased alloys, *Metall. Mater. Trans*., A 36, 1627-1641.

Delalondre, F., 2008, Simulation and 3-D analysis of adiabatic shear bands in high speed metal forming processes, *PhD Mines ParisTech*, Sophia-Antipolis, 243 (in French).

Ducloux, R., Barbelet, M., Fourment, L., 2013, Automatic optimization of a complete manufacturing chain, *NUMIFORM, AIP Conf. Proc*. 1532, 665-670.

Ejday, M., Fourment, L., 2010, Metamodel assisted multi-objective optimization for metal forming applications, *Mécanique & Industries*, 11, 3-4, 223-233.

El Khaoulani, R., Bouchard, P.-O., 2012, An anisotropic mesh adaptation strategy for damage and failure in ductile materials, *Finite Elements in Analysis and Design,* 59, 1-10.

Elsey, M., Esedoglu, S., Smereka, P., 2009, Diffusion generated motion for grain growth in two and three dimensions, *J. Comput. Phys*., 228*, 8015-8033.*

Fabiano, A.-L., Logé, R., Bernacki, M., 2014, Assessment of simplified 2D grain growth models from numerical experiments based on a level set framework, *Comp. Mater. Sci*., 92, 305-312.

Fourment, L., Chenot J. L., 1994, Adaptive remeshing and error control for forming processes, *Revue Européenne des Éléments finis*, 3, 2, 247-279.

Fourment, L., Chenot J. L., Mocellin K., 1999, Numerical formulations and algorithms for solving contact problems in metal forming simulation, *International Journal for Numerical Methods in Engineering*, 46, 9, 1435-1462.

Fourment, L., Popa, S., Barboza, J., 2004, A Quasi-Symmetric Contact Formulation For 3D Problems. Application To Prediction Of Tool Deformation In Forging, 8th International Conference on Numerical Methods in Industrial Forming Processes (NUMIFORM), Columbus, Ohio, AIP Conf. Proc. 712, 2240.

Fourment, L., 2007, Meta-model based optimisation algorithms for robust optimization of 3D forging sequences, in *10th ESAFORM Conference on Material Forming*, Pts A and B, E. Cueto and F. Chinesta, Editors, 21-26.

Fourment, L., 2008, A quasi-symmetric formulation for contact between deformable bodies, *European Journal of Computational Mechanics*, 17, 5-7, 907, 918.

Gachet, J.-M., Delattre, G., Bouchard, P.-O., 2014, Fracture mechanisms under monotonic and non-monotonic low Lode angle loading, *Engineering Fracture Mechanics*, 124-125, 121-141.

Galeao, A.C., Do Carmo, E. G. D., 1988, A consistent approximate upwind Petrov-Galerkin method for convection-dominated problems, *Computer Methods In Applied Mechanics and Engineering,* 68, 1, 83-95.

Hill, R., 1948, A theory of the yielding and plastic flow of anisotropic metals. *Proc. Roy. Soc*., London, 193, 281-297.

Hitti, K., Laure, P., Coupez, T., Silva, L., Bernacki, M., 2013, Precise generation of complex statistical Representative Volume Elements (REVs) in a finite element context*, Comp. Mater. Sci.,* 61, 224-238.

Gruau, C., Coupez, T., 3D tetrahedral, unstructured and anisotropic mesh generation with adaptation to natural and multidomain metric, *Comp. Meth in Appl. Mech and Engg*., 194, 48-49, 4951-4976.

Habraken, A.-M., Cescotto, S., 1998, Contact between deformable solids, the fully coupled approach, *Mathematical & Computer Modelling,* 28 (4-8), 153-169.

Hachem, E., Jannoun, G., Veysset, J., Henri, M., Pierrot, R., Poitrault I., Massoni E., Coupez T., 2013, Modeling of heat transfer and turbulent flows inside industrial furnaces, *Simulation Modelling Practice and Theory*, 30, 35-53.

Hallberg, H., 2013, A modified level set approach to 2D modeling of dynamic recrystallization, *Modelling Simul. Mater. Sci. Eng*., 21, 8, 085012.

Hallquist, J. O., Goudreau, G. L., Benson, D. J., 1985, Sliding interfaces with contact-impact in large-scale Lagrangian computations, *Comput. Meth. Appl. Mech. Engng*., 51, 1-3, 107-137.

Hirt, G., Kopp, R., Hofmann, O., Franzke, M., Barton, G., 2007, Implementing a high accuracy Multi-Mesh Method for incremental Bulk Metal Forming, *CIRP Annals-Manufacturing Technology*, 56, 313-316.

Iwata, K., Osakada, K., Fujino, S., 1972, Analysis of hydrostatic extrusion by the finite element method., *Transactions of the ASME*, B, 94-2, 697-703.

Jaouen, O., Costes, F., Barbelet, M., Lasne, P., 2014a, From continuous casting to rolling process simulation with a full 3D powerful software tool, *1st ESTAD & 31st JSI*, 7-8 April, Paris.

Jaouen, O., Costes, F., Lasne, P., Fourment, C., Barbelet, M., 2014b, Numerical simulation of a shell forming, from hollow ingot to the final product, with a powerful software tool, *2nd International Conference on Ingot Casting Rolling & Forging, ICRF2014,* Milano.

Jin, Y., Lin, B., Bernacki, M., Rohrer, G.S., Rollett, A.D., Bozzolo N., 2014, Annealing twin development during recrystallization and grain growth in pure nickel, *Material Sci. and Engg. A,* 597, 295-303.

Karma, A., 2001, Phase-Field Formulation for Quantitative Modeling of Alloy Solidification, *Phys. Rev. Lett.,* 87, 115701.

Kim, N., Machida, S., Koboyashi, S., 1990, Ring rolling process simulation by the three dimensional finite element method*, Int. J. Machine Tools and Manufacture*, 30, 569-577.

Khoei, A.R., Gharehbaghi, S.A., 2007, The superconvergence patch recovery technique and data transfer operators in 3D plasticity problems, *Finite Elements in Analysis and Design,* 43, 8, 630-648.

Ko, K.J., Cha, P.A., Srolovitz, D., Hwang, N.M., 2009, Abnormal grain growth induced by sub-boundary-enhanced solid-state wetting: Analysis by phase-field model simulations, *Acta Mater.*, 57, 838-845.

Kugler, G., Turk, R., 2004, Modeling the dynamic recrystallization under multi-stage hot deformation, *Acta Mater.,* 52, 15, 4659-4668.

Kumar, S., Fourment, L., Guerdoux, S., 2015, Parallel, second-order and consistent remeshing transfer operators for evolving meshes with superconvergence property on surface and volume, *Finite Elements in Analysis and Design,* 93, 70–84, DOI: 10.1016/j.finel.2014.09.002.

Launder, B. E., Spalding, D. B., 1974, The numerical computation of turbulent flows, *Computer Methods In Applied Mechanics And Engineering*, 3, 2, 269-289.

Lebon, J., Le Quillec, G., Breitkopf, P., Coelho, R. F., Villon, P., 2014, A two-pronged approach for springback variability assessment using sparse polynomial chaos expansion and multi-level simulations, *International Journal of Material Forming,* 7, 3, 275-287.

Lee, C. H., Kobayashi, S., 1973, New Solutions to Rigid-Plastic Deformation Problems Using a Matrix Method, *J. Eng. Ind.,* 95, 865.

Logé, R., Bernacki, M., Resk, H., Delannay, L., Digonnet, H., Chastel Y., Coupez T., 2008, Linking plastic deformation to recrystallization in metals using digital microstructures, *Philosophical Magazine B*, 88, 30-32, 3691-3712.

Mahajan, P., Fourment L, Chenot J.-L., 1998, Implicit scheme for contact analysis in non-steady state forming, *Engineering Computations*, 15, 6-7, 908-924.

Mesri, Y., Zerguine, W., Digonnet, H., Silva, L., Coupez, T., 2008, Dynamic parallel mesh adaption for three dimensional unstructured meshes: Application to interface tracking. *Proceeding of the 18th IMR*, Springer,195-212.

Militzer, M., 2011, Phase field modeling of microstructure evolution in steels, *Cur. Op. Solid St. Mater. Sci.*, 15, 106-115.

Moelans, N., Wendler, F., Nestler, B., 2009, Comparative study of two phase-field models for grain growth, *Comp. Mater. Sci*., 46, 479-490.

Mole, N., Chenot, J. –L., Fourment, L., 1996, A velocity based approach including acceleration to the finite element computation of viscoplastic problems*, Int. J. Numer. Methods Engng*., 39, 3439-51.

Mukherjee, M., Prahl, U., Bleck, W., 2010, Modelling of microstructure and flow stress evolution during hot forging, *Steel Research Int*., 81, 1102-1116.

Nagata, T., 2005, Simple local interpolation of surfaces using normal vectors, *Computer Aided Geometric Design,* 22, 327-347.

Nagai, T., Ohta, S., Kawasaki, K., Okuzono, T., 1990, Computer simulation of cellular pattern growth in two and three dimensions, *Phase Trans.,* 28, 177-211.

Nahshon, K., Hutchinson, J., 2008, Modification of the Gurson model for shear failure, *Eur. J. Mech. A/Solids*, 27, 1, 1-17.

Nédélec, J. C., 1986, A new family of mixed finite elements in R^3, *Numer. Math.,* 50, 57-81.

Page, D. L., Sun, Y., Koschan, A. F., Paik, J., Abidi, M. A., 2002, Normal Vector Voting: Crease Detection and Curvature Estimation on Large, Noisy Meshes, Graphical Models, 64, 199-229.

Osher, S., Sethian, J. A., 1988, Fronts propagating with curvature-dependent speed: Algorithms based on Hamilton–Jacobi formulations, *J. Comput. Phys.,* 79, 12-49, doi:10.1016/0021-9991(88)90002-2.

Piekos, K., Tarasiuk, J., Wierzbanowski, K., Bacroix, B., 2008a, Stochastic vertex model of recrystallization, *Comp. Mater. Sci*., 42, 1, 36-42.

Piekos, K., Tarasiuk, J., Wierzbanowski, K., Bacroix, B., 2008b, Generalized vertex model of recrystallization – Application to polycrystalline copper, *Comp. Mater. Sci.,* 42, 4, 584-594.

Ramadan, M., Fourment, L., Digonnet, H., 2009, A parallel two mesh method for speeding-up progresses with localized deformations: application to cogging*, Int. J. of Material Forming*, 2, Supplement 1, 581-584.

Resk, H., Delannay, L., Bernacki, M., Coupez, T., Logé, R.E., 2009, Adaptive mesh refinement and automatic remeshing in crystal plasticity finite element simulations, *Modelling Simul. Mater. Sci. Eng.,* 17, 075012.

Rey, B., Mocellin, K., Fourment, L., 2008, A node-nested Galerkin multigrid method for metal forging simulation, *Computing and Visualization in Science*, 11, 1, 17-25.

Rollett A.D., Raabe D., 2001, A hybrid model for mesoscopic simulation of recrystallization, *Comput. Mater. Sci.,* 21, 69-78.

Roux, E., 2011, Mechanical joining- Process optimization strategies and identification of materials mechanical behaviors, *PhD at Ecole des Mines de Paris*, Sophia Antipolis (in French).

Roux, E., Bouchard, P.-O., 2011, Numerical investigation of ductile damage parameters identification: benefit of local measurements, A. J. Kassab, E. A. Divo Editors, *the 7th International Conference on Inverse Problems in Engineering (ICIPE),* May 2011, Orlando, United States. Centecorp Publishing, 221-226.

Roux, E., Bernacki, M., Bouchard, P.-O., 2013, A level set and anisotropic adaptive remeshing strategy for the modeling of void growth under large plastic strain, *Computational Materials Science,* 68, 32-46.

Roux, E., Shakoor, M., Bernacki, M., Bouchard, P.-O., 2014, A new finite element approach for modelling ductile damage void nucleation and growth – analysis of loading path effect on damage mechanisms, *Modelling Simul. Mater. Sci. Eng.,* 22, 075001, doi:10.1088/0965-0393/22/7/075001.

Ryckelynck, D., 2009, Hyper-reduction of mechanical models involving internal variables, *Int. J. Numer. Meth. Engng.,* 77, 1, 75-89.

Saby, M., Bernacki, M., Roux, E., Bouchard, P.-O., 2013, Three-dimensional analysis of real void closure at the meso-scale during hot metal forming processes, *Computational Materials Science,* 77, 194-201.

Saby, M., Bernacki, M., Bouchard, P.-O., 2014, Understanding and modeling of void closure mechanisms in hot metal forming processes: a multiscale approach, *11th International Conference on Technology of Plasticity, ICTP,* 19-24 October 2014, Nagoya Congress Center, Nagoya, Japan.

Sethian, J.A., 1996, Level Set Methods, *Cambridge University Press*, Cambridge.

Song, G., Bjorge, T., Holen, J., Magnussen, B. F., 1997, Simulation of fluid flow and gaseous radiation heat transfer in a natural gas-fired furnace, *International Journal of Numerical Methods for Heat and Fluid Flow*, 7, 169-182.

Strano, M. A, 2008, Technique for FEM optimization under uncertainty of time-dependent process variables in sheet metal forming, *Int. J. Mater. Form.,* 1, 13-20.

Surdon, G., Chenot, J.-L., 1987, Finite element calculation of three-dimensional hot forging, *Int. J. Numer. Meth. Eng*., 24, 2107-2117.

Syha, M., Weygand, D., 2010, A generalized vertex dynamics model for grain growth in three dimensions, *Modelling Simul. Mater. Sci. Eng*., 18, 015010.

Takaki, T., Hisakuni, Y., Hirouchi, T., Yamanaka, A., Tomita, Y., 2009, Multi-phase-field simulations for dynamic recrystallization, *Comput. Mater. Sci.,* 45, 881-888.

Teodorescu, M., Lasne, P., Logé, R., 2007, Modeling recrystallization for 3D multi-pass forming processes, *Materials Science Forum*, 558-559, 1201-1206.

Traore, K., Forestier, R., Mocellin, K., Montmitonnet, P., Souchet M., 2001, Three dimensional finite element simulation of ring rolling, *Proc. of the 7th International Conference on Numerical Methods in Industrial Forming Processes NUMIFORM 2001*, ed. by K. Mori, A. A. Balkema, 595-600.

Wagoner, R. H., Chenot, J.-L., 2001, Metal forming analysis, *Cambridge University Press,* Cambridge.

Wang, C., Liu, G., 2003, On the stability of grain structure with initial Weibull grain size distribution, *Mater. Lett*., 57, 28, 4424-4428.

Wiebenga, J. H., Weiss, M., Rolfe, B., Van Den Boogaard, A. H., 2013, Product defect compensation by robust optimization of a cold roll forming process, *Journal of Materials Processing Technology,* 213, 6, 978-986.

Weygand, D., Brechet, Y., Lepinoux, J., 2001, A vertex simulation of grain growth in 2D and 3D, *Adv. Eng. Mater.,* 3,1-2, 67-71.

Xu, T., Li, M., 2009, Topological and statistical properties of a constrained Voronoi tessellation, *Phil. Mag.,* 89, 349-374.

Zabaras, N., Bao, Y., Srikanth, A., Frazier, W. G., 2000, A continuum Lagrangian sensitivity analysis for metal forming processes with applications to die design problems, *Int. J. Numer. Meth. Engng,* 48, 679-720.

Zienkiewicz, O. C., Godbole, K., 1974, Flow of Plastic and Visco-Plastic Solids with Special Reference to Extrusion and Forming Processes, *Int. J. Numer. Meth. Eng.,* 8, 1, 1-16.

Zienkiewicz, O.C., Zhu J.Z., 1992, The superconvergent patch recovery (SPR) and adaptive finite element refinement, *Computer Methods in Applied Mechanics and Engineering*, 101, 207-224.

AKTUALNY I PRZYSZŁY ROZWÓJ SYMULACJI METODĄ ELEMENTÓW SKOŃCZONYCH PROCESÓW PRZERÓBKI PLASTYCZNEJ METALI

Streszczenie

Po ponad 40 latach rozwoju metoda elementów skończonych (MES) osiągnęła wysoki poziom doskonałości. W artykule przedstawiono krótki wstęp do rozwiązywania tą metodą zadań mechanicznych i cieplnych, a następnie opisano główne naukowe i techniczne aspekty rozwoju MES. Rozważono problemy numeryczne, takie jak adaptacyjna przebudowa siatki (adaptive remeshing), rozwiązywanie zadań sprzężonych, takich jak sprzężenie cieplno-mechaniczne, dla otrzymania bardziej realistycznych symulacji. Duży nacisk położono też na modelowanie rozwoju mikrostruktury, zastosowanie metod optymalizacji procesów kształtowania metali oraz na identyfikację parametrów modeli. W końcowej części artykułu omówiono główne potencjalne kierunki badań przewidywanych na najbliższe 10 lat, obejmujących stabilizację rozwiązania, uwzględnienie aspektów stochastyczne oraz bardziej efektywne obliczenia rozproszone. Podsumowaniem jest propozycja rozszerzenia zastosowań MES i stworzenie „wirtualnej fabryki".

Received: January 5, 2014
Received in a revised form: March 13, 2015
Accepted: March 30, 2015